POLITECNICO DI MILANO
Master's in Space Engineering
Department of Aerospace Engineering
School of Industrial and Information Engineering

LIBRATION POINT ORBIT STATION-KEEPING: CONTROL STRATEGIES FOR IMPROVED SCIENTIFIC MISSION TIME

Supervisor: Prof. James Douglas Biggs

MSc. Thesis by:
Lorenzo Guerreschi
Matricola Id: 916192

Academic Year 2019/2020

Acknowledgment

I would like to thank Professor James Douglas Biggs for his patience during the thesis work. His continuous help in providing hints and suggestions on every step of the work has been fundamental for the completion of this final task.
I would like also to thank the Politecnico institute and all the professors and colleagues I have met. They have helped and influenced my growth in all the years of the bachelor and master degree courses.

Abstract

The scientific interest in the exploitation of Lagrangian points orbits has increased in the last decades. The requirement of precise station-keeping for the unstable motion of Halo orbits has brought many control techniques. In addition, the use of Cubesats has the potential to reduced mission cost. The primary task of a space mission is subject to its scientific requirements, which are not generally considered by the classical control schemes. For example, optimal controls typically aim to minimize fuel and tracking error, it may also be desirable to maximise the time at which science can be undertaken. Moreover, during station-keeping maneuvers it may not be possible to perform the science, since the thrust-vectoring required may be in a different direction to the payload pointing requirement. This thesis presents the development of controls that are able to combine stable station-keeping and maximize the time where no control is required. The Elliptical Restricted 3-Body Problem and a simple Linear Quadratic Regulator are introduced, capable of providing continuous control. This classic control algorithm is augmented to include impulsive control, coupled with different strategies. The performance of these strategies is analysed with respect to delta-V, tracking error and time for science.

List of Figures

List of Tables

Contents

Chapter 1

Introduction

1.1 Motivation

The orbits around Lagrangian points have attracted the mission analyst because they provide natural orbits of strategic importance, with theoretically fuel-free trajectories. However, due to their inherent instability, they require station-keeping. The existence of Lagrange points in the restricted three body problem has been known since the mid-eighteen century. The real importance of these special locations in the solar system became clear in the Space Age of 1960's. It was immediately evident that several missions could be accomplished only by the use of these points. The first space mission that placed a spacecraft in a Lagrange point was the International Sun-Earth Explorer-3 (ISEE-3), whose selected location was the Sun-Earth L1 point, a suitable location for an obstructed view of the Sun. Scientific missions where instead its presence was undesirable where placed in the L2 points, such as the Wilkinson Microwave Anisotropy Probe (WMAP). In the Earth-Moon system, the L2 point provides a suitable place for continuous relay communication, a feature that have been exploited by the Chang'e 4 mission through the Queqiao relay satellite. A future mission that would exploit this point for scientific purpose is the Lunar Meteoroid Impact Observer (LUMIO), thanks to the continuous and unobstructed view of the Moon far side. The L1 Earth-Moon Lagrange point is instead a suitable

location for a space station and Nasa is currently developing the Lunar Gateway, whose final orbit will be a highly elliptical near-rectilinear halo orbit.

As miniaturization technology is improving [22], it seems beneficial to use the newly developed Cube-sat standard. The advantage of such technology, starting from lower price and reliability requirements, is that a Cube-Sat could have a ride-share with a bigger and more complex payload, therefore with no need to define a separate mission.

Of course, it is expected that a Cube-sat mission would mostly be dedicated to its scientific payload, which may have specific requirements about pointing and time schedule. It is therefore mandatory that the Cube-sat is able to meet said scientific requirements, while also being able to maintain its given orbit through station-keeping maneuvers.

It is therefore clear that a continuous control algorithm, which would be continuously active, can not provide spare time for its scientific mission.

1.2 Problem Statement

Scope of the thesis is to find, study and assess the performance of different control algorithms and strategies in order to reduce the portion of mission time dedicated to station-keeping procedures in L2 halo orbits, with the application of current propulsion technologies for miniaturized spacecrafts, namely chemical and electric propulsion.

In order to understand the problem definition for this mission, a brief review about the circular restricted three-body problem is firstly given. With this problem setup, a linear quadratic regulator (LQR) is introduced together with different control strategies to achieve impulsive control and suitably long windows of no station-keeping maneuvers.

In order to develop a more realistic scenario, it has been chosen to introduce in the simulation the data related to two commercially available thruster, a chemical and an electric one, in the form of available thrust. The choice of two different

propulsion unit is not meant to compare the two propulsion technologies but to find the suitable control algorithms that better suit the particular thruster.

1.3 Previous Work

Centuries ago Euler, Lagrange, and Jacobi introduced the dynamics of the Lagrangian points. The Jacobi integral forms an important part for a discussion of the transfer trajectories to these locations from Earth and vice-versa.

In the 1960s, Steg and Michael provided analysis of the stability of triangular regions studying the motion of a particle placed at the Earth-Moon L4 location. They investigated the influence of third body perturbations and extended it to the elliptical lunar orbit. However, due to the limitation of numerical calculus at the time, the search of periodic orbits was significantly limited and it was believed by Forest and Moulton that certain periodic solutions are practically impossible to compute. With the invention of computers and calculators such concern was gone, and numerical procedures paved the way for several types of periodic solutions.

Poincarè first indicated periodic solutions as the primary mean of understanding the CR3BP [20][39]. Howell and Keeter [25] also studied the orbits in these locations of E-M system. Many periodic orbits have been successfully exploited for space mission applications in both the Sun-Earth and Earth-Moon [24] system. Catalogs of quasi-periodic orbits have been compiled to better understand the dynamical behaviour [23] and guide the mission design within the context of a given three-body system. Farquhar [11] and Hoffman provided analysis and discussion of stability and control of the Earth-Moon co-linear L2 and L1 locations, respectively, in a classical control theory. Howell and Folta [15] detailed an analysis of transfers between the Sun-Earth locations and the Earth-Moon locations. The effects of the various perturbation with respect to orbits in the vicinity of moon were studied by Martin T. Ozimek [36] in his PhD dissertation. Later, Wong, Patil and Misra detailed about the effects of gravity torque along Lagrangian point orbits for a single, rigid vehicle in the Sun-Earth system [50]. Howell identified the initial conditions for periodic orbits

around Lagrangian point. This was followed by Folta [15] where he has dealt with Earth-Moon Lagrangian station-keeping. Gordon [18] aid in the numerical procedure for the station-keeping methodologies around Lagrangian point trajectories including error analysis. Grebow identified the important orbits and the station-keeping requirements for the particular case of south pole coverage [19].

The full three-dimensional coupled motion was explored by Knutson and Howell [28] for a multiple spacecraft flight in non-linear Lyapunov and halo reference orbits. Periodic solutions are typically generated by numerically correcting an initial guess to meet specific boundary conditions, which include the continuity between the final and initial states. This numerical procedure have been referred to as "Differential Corrector" [29] and has been widely used in previous work on Lagrangian point orbits. Even with the current computational capabilities, the convergence of algorithms for periodic orbits depends significantly on the accuracy of the initial guess and the implementation of the targeting scheme.

To simulate a real scenario of the E-M Lagrange points, it is important to find natural Lagrangian orbits. Thus, an elliptical problem is important to be considered in the trajectory definition. Campagnola [7] introduced the formulation of elliptical restricted three body problem in the most simpler form such that they could be reduced to CR3BP when e = 0.

For what concerns control, instead, the Lagrangian point orbits are naturally unstable, but controllable. Additional control force is therefore needed for a spacecraft to remain close to its nominal orbit. The challenges of station-keeping control emerge from high accuracy, low computational burden and minimal fuel cost requirements under the condition of dynamic uncertainties, unmodelled perturbations, and initial orbit injection errors [43]. Hence, station-keeping control for libration point is vital but posses a great number of difficulties.

The study of station-keeping control on libration point orbits has become a popular research topic ever since the problem was firstly proposed. A vast majority of the station-keeping control methods are designed based on LTI model via local linearization at the libration points due to the high non-linearity of the dynamic equation of libration point orbits. There are numerous references for the discussion of stability

and control for both co-linear and triangular locations. Farquhar and Hoffman provided analysis and discussion of stability and control of the Earth-Moon co-linear L2 and L1 locations, respectively, in a classical control theory. Cielaszyk and Wie [8] employed a new LQR control method combined with a disturbance accommodating controller for Lissajous and Halo orbits maintenance based on LTI model. Howell and Pernicka [26] developed a target-point approach to maintain the spacecraft within a region about the nominal Halo orbit. Furthermore, several other control strategies have been developed: Kulkarni et al. [30] extended the traditional framework to periodic, discrete LTV systems for spacecraft flight stabilization in Halo orbits, Wang et al. [48] presented a nonlinear controller based on polynomial eigen-structures of LTV model for the control of Sun-Earth point station-keeping and Rahmani et al. [41] solved the problem of Halo orbit control using optimal control theory and the variation of the extreme technique. Biggs et al. [4] enhanced the station-keeping control with the use of an extended state observer

However, the robustness under nonlinear system uncertainties and the request for low computational burden are not always investigated. Oguri et al. [36] developed a station-keeping procedure that included different sources of error and tested it using a Montecarlo simulation. The same procedure was used by Narula [34]. The computational burden was instead investigated by Kim and Hall [27], who also provided a user-friendly interface for a periodic orbit generator. Han [21] introduced an active disturbance rejection station-keeping control method proposing an error driven, rather than model-based control law which takes into account system uncertainties, unmodelled disturbance, and orbit injection errors to achieve better robustness. This could achieve a better station-keeping performance as well as a smaller computational effort.

Moreover, few of these works have dealt with the problem related to the scientific mission requirements. The discussions involved optimal control and discontinuous control, for single and multiple spacecraft around Lagrangian points, without assessing the performance of their control under the point of view of reducing control active time. The work developed by Oguri et al. [36] and Garulli et al. [16] provided a station-keeping algorithm that allows discontinuous control, therefore suitable for

a scientific application, but with no explicit declaration of this concept. The idea of discontinuous thrust was investigated also by Eckstein [9], where he also carried the case of an electric propulsion system under given limitations on thrust magnitude and operation times. Both concepts are studied in this thesis work. Table 1.1 presents different control techniques and their relevant features.

Control Method	**Features**	**Ref.**
Convex optimization problem	robust and optimized	43
Target point and Floquet mode	Impulsive	26
H_∞ approach	discrete control	30
Polynomial eigenstructure assignment	continuous and optimized	48
Optimal control theory	optimized	41
Extended state observer	continuous	4
Time continuation of quasi halo orbits	impulsive	36
Active disturbance rejection control	continuous	21
Extended Kalman filter	hybrid continuous/impulsive	16
Optimization techniques	impulsive and optimized	9
Time-delayed feedback control	continuous	6

Table 1.1: Control techniques and relevant features

1.4 Structure of the Thesis

The thesis is organized in the following structure.

Chapter 2 introduces the orbital dynamic frame which is is used to simulate the motion of a third body in the Earth-Moon system. Starting from the assumptions and the reference frame used, the equations of motion are derived firstly for the circular restricted problem, and then for the elliptical restricted problem. Then, the concept of state transition matrix is introduced and used to compute periodic orbits.

Chapter 3 shows how to transform a periodic orbit into a reference trajectory for a control algorithm. Then, the construction of a Linear Quadratic Regulator

is explained. After a brief introduction of the main control algorithms, different methodologies to obtain a control that simultaneously achieves stable station keeping and time windows where no control is required are explained.

Chapter 4 is introduced by the other details that complete the simulation environment, from disturbances and errors to performance criteria and thruster selection. Then, the results of the various trajectory and control algorithms are listed.

Chapter 5 is dedicated to the conclusion of the thesis work and the lessons learned, together with possible ideas for future works.

Chapter 2

Orbital Dynamics

This chapter is dedicated to the review of important mathematical and physical concepts relevant to this work. The difference between different reference frames is introduced and the equations of motions are developed first for the Circular Restricted 3-Body Problem (CR3BP) and then extended to the Elliptical Restricted 3-Body Problem (ER3BP) with the addition of eccentricity of the secondary in the equation of motion. The concept of differential corrector is introduced and particular solutions, such as equilibrium points, as well as periodic orbits are discussed. The dynamics is then solved for the problem to define the initial condition of unstable Lagrange point orbit.

The refined initial conditions will be used in Chapter 3 in order to provide reference trajectories for a suitable control algorithm, capable of providing station-keeping.

2.1 Circular Restricted 3-Body Problem

The simplest formulation of the mutual gravitational interaction between three point-mass bodies consists in the Circular Restricted 3-Body Problem. The motion of the third body moves under the gravitational attraction of the two primaries, constrained to move on circular orbits around the system center of mass, without influencing their

motion. Such model is valid when the mass of the third body is negligible compared to that of the primaries.

2.1.1 Equation of Motion

Following the procedure found in [35], the derivation of the equations of motion in the three-body problem begins with a set of n particles. From the inverse-square law of gravity, the force on a particle i due to a particle j is:

$$\overrightarrow{F}_i = -\frac{Gm_i m_j}{r_{ji}^3}\overrightarrow{r}_{ji} \tag{2.1}$$

where G is the gravitational constant, m_i and m_j are the masses of the two particles and $\overrightarrow{r}_{ji}$ is their distance vector.

Since:

$$\overrightarrow{F}_i = m_i \ddot{\overrightarrow{r}}_i \tag{2.2}$$

equation 2.1 can be rewritten as:

$$\ddot{\overrightarrow{r}}_i = -\frac{Gm_j}{r_{ji}^3}\overrightarrow{r}_{ji} \tag{2.3}$$

If more particles were present, then acceleration of particle i could be written as:

$$\ddot{\overrightarrow{r}}_i = \sum_{j=1}^{n-1} -G\frac{m_j}{r_{ji}^3}\overrightarrow{r}_{ji} \tag{2.4}$$

The undergoing problem requires $n = 3$, therefore, for a three body problem, the inertial acceleration of the spacecraft due to the other two bodies is given as:

$$\ddot{\overrightarrow{r}}_3 = -\frac{Gm_1}{r_{13}^3}\overrightarrow{r}_{13} - \frac{Gm_2}{r_{12}^3}\overrightarrow{r}_{12} \tag{2.5}$$

The next step consists in transforming the inertial reference frame into a rotating one, with constant angular velocity equal to the mean Moon orbital angular velocity n. True anomaly follows the equation $\theta(t) = nt$.

The Inertial reference frame is valid for the equations of motion as defined above by Newton's laws. This inertial frame is centered on the barycenter of the system,

the X is directed towards the right side from the barycenter and will cross the moon when they are in same alignment. The Y axis is directed perpendicular upwards as shown in the figure 2.1. The Z-axis is coming out of the plane towards the reader.

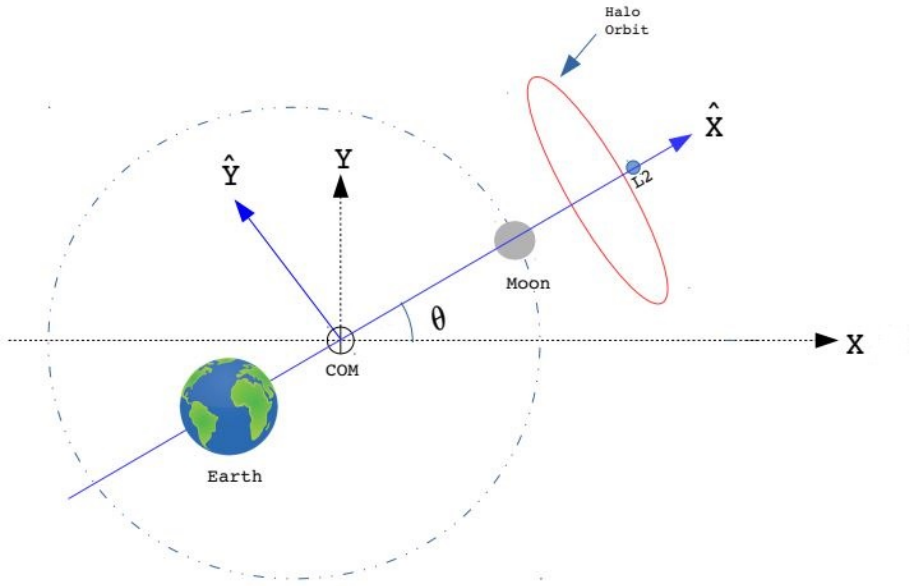

Figure 2.1: Comparison between Inertial and Rotating reference frames [35]

The Rotating reference frame is the best visualisation of three-body problem where the spacecraft is moving near the Lagrangian points. The barycenter of the system is again the origin of this new reference. The vector $\hat{X}$ is defined such that it is directed from the barycenter towards the small primary. The $\hat{Y}$ axis is 90^o from $\hat{X}$ in the plane of the motion of the primaries. The vector $\hat{Z}$ completes the triad and is normal to the plane of motion.

Before this transformation, however, it's useful to write equation 2.5 using normalized quantities. Normalization is performed by proper characteristic quantities that depend on the particular analyzed system (in this case, the Earth-Moon system). This provides an advantage for the numerical and computational point of view. The characteristic quantities are:

- $l^* = a$, where a is the Moon semi-major axis (384,748 km)

- $m^* = m_1 + m_2$, where m_1 and m_2 are Earth and Moon mass, respectively
- $t^* = \sqrt{\frac{(l^*)^3}{Gm^*}} = 375,704s$

Using these quantities, the mass of the two primaries can be written as:

$$\mu = \frac{m_2}{m^*} \tag{2.6}$$

for the second primary, and

$$1 - \mu = \frac{m_1}{m^*} \tag{2.7}$$

for the first one, while the distances between the spacecraft and the two bodies become:

$$\overrightarrow{r} = \frac{\overrightarrow{r}_{23}}{l^*} \tag{2.8}$$

and

$$\overrightarrow{d} = \frac{\overrightarrow{r}_{13}}{l^*} \tag{2.9}$$

It is worth noting that in the rotating reference frame the coordinates of the two primaries are (-μ,0,0) for the Earth and (1-μ,0,0) for the Moon. Moon orbital Angular velocity, in turn, becomes:

$$n = \frac{2\pi}{T} * t^* = 1 \tag{2.10}$$

where T is Moon sidereal period. Time, too, changes, and becomes:

$$\tau = \frac{t}{t^*} \tag{2.11}$$

so that $t = T$ is represented as $\tau = 2\pi$ in the model with normalized quantities. Also, the value of G has been imposed to be equal to 1. With these considerations, equation 2.5 becomes:

$$\ddot{\overrightarrow{\rho}} = -\frac{1-\mu}{d^3}\overrightarrow{d} - \frac{\mu}{r^3}\overrightarrow{r} \tag{2.12}$$

Applying a rotation with constant angular velocity n to

$$\overrightarrow{\rho} = \begin{bmatrix} \rho_x \\ \rho_y \\ \rho_z \end{bmatrix} \tag{2.13}$$

it can be obtained that

$$\begin{bmatrix} \rho_x \\ \rho_y \\ \rho_z \end{bmatrix} = \begin{bmatrix} x \\ y \\ z \end{bmatrix} \tag{2.14}$$

where x,y,z are the components of the position vector in the rotating reference frame. By differentiating the kinematics, it derives that:

$$\begin{bmatrix} \dot{\rho}_x \\ \dot{\rho}_y \\ \dot{\rho}_z \end{bmatrix} = \begin{bmatrix} \dot{x} - y \\ \dot{y} + x \\ \dot{z} \end{bmatrix} \tag{2.15}$$

$$\begin{bmatrix} \ddot{\rho}_x \\ \ddot{\rho}_y \\ \ddot{\rho}_z \end{bmatrix} = \begin{bmatrix} \ddot{x} - 2\dot{y} - x \\ \ddot{y} + 2\dot{x} - y \\ \ddot{z} \end{bmatrix} \tag{2.16}$$

therefore, equation 2.5 can be rewritten in the rotating reference frame as:

$$\begin{aligned} \ddot{x} - 2\dot{y} - x &= -\frac{(1-\mu)(x+\mu)}{d^3} - \frac{\mu(x-(1-\mu))}{r^3} \\ \ddot{y} + 2\dot{x} - y &= -\frac{(1-\mu)y}{d^3} - \frac{\mu y}{r^3} \\ \ddot{z} &- \frac{(1-\mu)z}{d^3} - \frac{\mu z}{r^3} \end{aligned}$$

while vectors $\overrightarrow{d}$ and $\overrightarrow{r}$ can be rewritten as:

$$\begin{aligned} \overrightarrow{d} &= (x-(-\mu))\hat{X} + y\hat{Y} + z\hat{Z} \\ \overrightarrow{r} &= (x-(1-\mu))\hat{X} + y\hat{Y} + z\hat{Z} \end{aligned}$$

This set of Ordinary Differential Equations represents spacecraft motion in the Rotating reference frame for the CR3BP.

2.1.2 Lagrange Points

The ODE of motion can be used to locate Lagrange points in the Rotating reference. In 1772, Lagrange identified these points for a restricted 3-body problem with the

assumption of circular orbits. The L1, L2 and L3 are collinear equilibrium points and L4 and L5 are equilateral Lagrangian points. These points are obtained by equating:

$$-x_{eq} = -\frac{(1-\mu)(x_{eq}+\mu)}{d_{eq}^3} - \frac{\mu(x_{eq}-(1-\mu))}{r_{eq}^3}$$
$$-y_{eq} = -\frac{(1-\mu)y_{eq}}{d_{eq}^3} - \frac{\mu y_{eq}}{r_{eq}^3}$$
$$z_{eq} - \frac{(1-\mu)z_{eq}}{d_{eq}^3} - \frac{\mu z_{eq}}{r_{eq}^3}$$

L1, L2, L3 can be found by assuming $y_{eq} = 0$, $z_{eq} = 0$, while L4, L5 require only $z_{eq} = 0$. Their location is listed in table 2.1

Lagrange Point	**Location**
L1	$-\mu < x_{eq} < 1-\mu$
L2	$x_{eq} > 1-\mu$
L3	$x_{eq} < -\mu$
L4	$x_{eq} = \frac{1}{2}, y_{eq} = \frac{\sqrt{3}}{2}$
L5	$x_{eq} = \frac{1}{2}, y_{eq} = -\frac{\sqrt{3}}{2}$

Table 2.1: Lagrange Points position

The Lagrangian of the CR3BP does not depend on time explicitly, which results in a constant Hamiltonian. It follows that the system possesses a constant of integration known as the Jacobi Constant. Physically, the gravitational forces must be balanced by the centrifugal forces. It follows that a modified potential energy function corresponding to the differential equations can be identified:

$$U = \frac{1}{2}(\dot{x}+\dot{y})^2 + \frac{1-\mu}{d} + \frac{\mu}{r} \tag{2.17}$$

The Jacobi constant, also know as 'integral of relative energy', is defined in terms of pseudo-potential as:

$$J_c = 2U - (\dot{x}^2 + \dot{y}^2 + \dot{z}^2) \tag{2.18}$$

Which allows to produce zero-velocity curves that identify the region of exclusion for a specific energy level. An example of such zero-velocity plot for Earth-Moon system is shown in figure 2.2

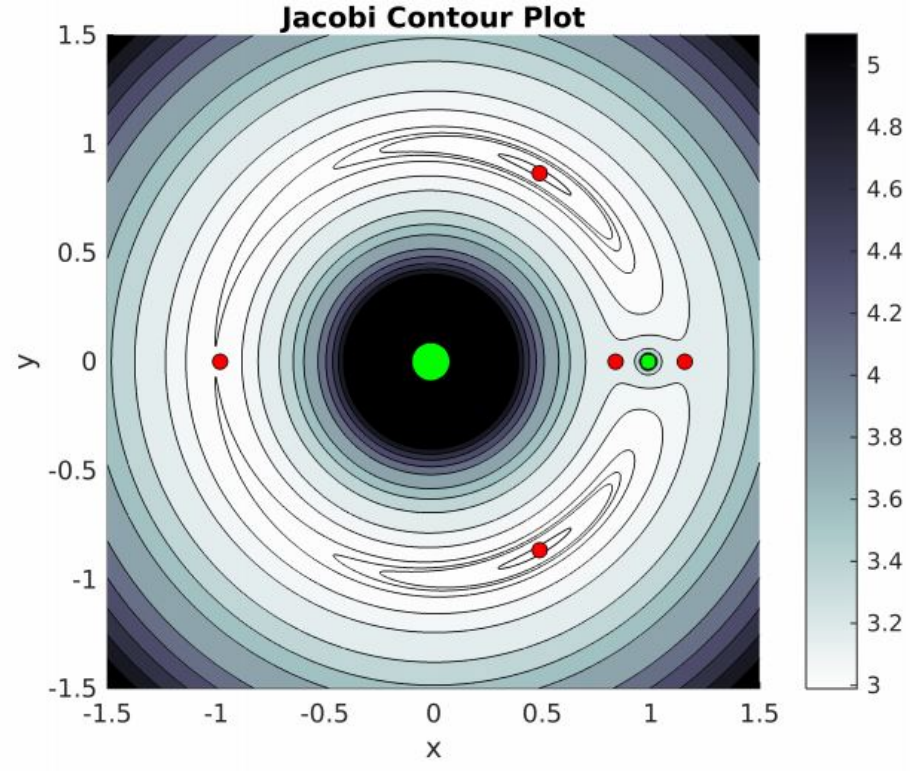

Figure 2.2: Zero-velocity curves [35]

2.1.3 State Transition Matrix

State transition matrix associated with the equation of motion is required by a differential correcting scheme. The STM provides the evolution of state vectors in time and this methodology is used to compute the nominal orbits of interest. It is generally denoted as $\phi(t, t_0)$ and is composed by the partial derivatives $\frac{\partial \vec{x}(t)}{\partial \vec{x}(t_0)}$ evaluated along the trajectory. The state vector is defined as $X = [x, y, z, \dot{x}, \dot{y}, \dot{z}]^T$.

In order to propagate STM, the following differential equation is evaluated:

$$\frac{d}{dt}\phi(t, t_0) = A(t)\phi(t, t_0) \tag{2.19}$$

with initial condition $\phi(t_0, t_0) = I_{6x6}$, where A is given by:

$$A(t) = \begin{bmatrix} \mathbf{0}_{3x3} & \mathbf{I}_{3x3} \\ \mathbf{U}_{dd} & 2\boldsymbol{\Omega} \end{bmatrix} \tag{2.20}$$

A is the matrix of the state-space representation of the ODE set of motion $\dot{X}(t) = \mathbf{A}(t)X(t)$, since the ODE set can be rewritten, using 2.17, into:

$$\begin{aligned} \ddot{x} &= \frac{\partial U}{\partial x} + 2\dot{y} \\ \ddot{y} &= \frac{\partial U}{\partial y} - 2\dot{x} \\ \ddot{z} &= \frac{\partial U}{\partial z} \end{aligned}$$

Matrix Ω is defined as:

$$\Omega = \begin{bmatrix} 0 & 1 & 0 \\ -1 & 0 & 0 \\ 0 & 0 & 0 \end{bmatrix} \tag{2.21}$$

and matrix U_{dd} is the 3x3 symmetric matrix containing the double partial derivatives of potential energy U:

$$U_{dd} = \begin{bmatrix} \frac{\partial^2 U}{\partial x^2} & \frac{\partial^2 U}{\partial x \partial y} & \frac{\partial^2 U}{\partial x \partial z} \\ \frac{\partial^2 U}{\partial y \partial x} & \frac{\partial^2 U}{\partial y^2} & \frac{\partial^2 U}{\partial y \partial z} \\ \frac{\partial^2 U}{\partial z \partial x} & \frac{\partial^2 U}{\partial z \partial y} & \frac{\partial^2 U}{\partial z^2} \end{bmatrix} \tag{2.22}$$

where each terms is defined as:

$$
\begin{aligned}
U_{xx} &= 1 - \frac{1-\mu}{d^3} - \frac{\mu}{r^3} + 3\frac{(1-\mu)(x+\mu)^2}{d^5} + 3\frac{\mu(x-1+\mu)^2}{r^5} \\
U_{yy} &= 1 - \frac{1-\mu}{d^3} - \frac{\mu}{r^3} + 3\frac{(1-\mu)y^2}{d^5} + 3\frac{\mu y^2}{r^5} \\
U_{zz} &= \frac{1-\mu}{d^3} - \frac{\mu}{r^3} + 3\frac{(1-\mu)z^2}{d^5} + 3\frac{\mu z^2}{r^5} \\
U_{xy} &= U_{yx} = 3\frac{(1-\mu)(x+\mu)y}{d^5} + 3\frac{\mu(x-1+\mu)y}{r^5} \\
U_{xz} &= U_{zx} = 3\frac{(1-\mu)(x+\mu)z}{d^5} + 3\frac{\mu(x-1+\mu)z}{r^5} \\
U_{yz} &= U_{zy} = 3\frac{(1-\mu)yz}{d^5} + 3\frac{\mu yz}{r^5}
\end{aligned}
$$

Having $\phi(t, t_0)$, it is possible to solve the variational equation

$$\dot{\delta\overrightarrow{x}} = \mathbf{A}(t)\delta\overrightarrow{x} \tag{2.23}$$

which has solution in the form

$$\delta\overrightarrow{x}(t) = \phi(t, t_0)\delta\overrightarrow{x}(t_0) \tag{2.24}$$

and where

$$\delta\overrightarrow{x}(t) = X(t) - X_{ref}(t) \tag{2.25}$$

where X_{ref} is the state space representation of the reference orbit. The solution represents the evolution of the initial error along the trajectory, and is fundamental in the computation of a suitable initial condition for a halo periodic orbit. This task requires the coupling of the 6 ODEs from orbital motion with the 36 ODEs coming from the STM.

2.1.4 Orbit Generation

The generation of orbits in CR3BP is a critical step towards the construction of an optimal reference for station-keeping. The sensitivity of this problem is quite high, but it is easily solvable.

As the main goal is to have a closed bounded periodic orbit near a co-linear Lagrangian point, initial condition of these orbits needs to be selected in such a way that it excites only stable modes associated with it.

The definition for a periodic orbit is given by Grebow[19] specified that the following conditions needs to be satisfied in order to call an orbit a periodic orbit:

- They should be symmetric about the x-z plane
- They should intersect the x-axis twice per orbit

The initial state vector is defined with the following notation:

$$\overrightarrow{X}_0 = [x_0, y_0, z_0, \dot{x}_0, \dot{y}_0, \dot{z}_0]^T \tag{2.26}$$

This initial condition can be strategically chosen such that it lays on the x-z plane with initial velocity only in the y-direction, therefore perpendicular to the x-z plane. Thus, the initial state will only have three components different from zero:

$$\overrightarrow{X}_0 = [x_0, 0, z_0, 0, \dot{y}_0, 0]^T \tag{2.27}$$

The requirement states that the orbit needs to be periodic about the x-z plane every time it crosses it. The next crossing should therefore occur after $t = \frac{T}{2}$, where T is the orbit period, and should be perpendicular again to the same plane:

$$\overrightarrow{X}_t = [x_t, 0, z_t, 0, \dot{y}_t, 0]^T \tag{2.28}$$

Given an initial condition, it is not guaranteed that this condition will happen, therefore the initial condition requires an adjustment, which can be provided by the solution of the variational equation.

Since the form of $\overrightarrow{X}_t$ is known, $\delta\overrightarrow{x}_t$ can be constructed as:

$$\delta\overrightarrow{x}_t = [0, 0, 0, \delta\dot{x}_t, 0, \delta\dot{z}_t]^T \tag{2.29}$$

which collects every term that make the crossing not perpendicular. After the solution of the STM 36 ODE set, $\phi(t, t_0)$ can be recovered and thus $\delta\overrightarrow{x}_0$ can be computed, which can be used to adjust the initial condition:

$$\overrightarrow{X}_{0,new} = \overrightarrow{X}_{0,old} - \delta\overrightarrow{x}_0 \tag{2.30}$$

A good strategy consists in computing $\delta\overrightarrow{x}_0$ in such a way that said adjustment doesn't alter perpendicularity property of the initial condition. In order to achieve this, the adjustment should be applied only to the non-zero condition:

$$\delta\overrightarrow{x}_0 = [\delta x_0, 0, \delta z_0, 0, \delta\dot{y}_0, 0]^T \tag{2.31}$$

It is also possible to impose the correction only to z_0, $\dot{y}_0$, so that:

$$\delta\overrightarrow{x}_0 = [0, 0, \delta z_0, 0, \delta\dot{y}_0, 0]^T \tag{2.32}$$

With this considerations, equation 2.24 can be inverted in order to find $\delta\overrightarrow{x}_0$:

$$\delta\overrightarrow{x}(t_0) = \phi(t, t_0)^\dagger \delta\overrightarrow{x}(t) \tag{2.33}$$

where † corresponds to the pseudo-inverse operation. The correction procedure requires the repetition of the computation for a suitable number of times. To ease the computation of the pseudo-inverse, equation 2.33 can be rewritten as:

$$\begin{bmatrix}\delta z_0 \\ \delta\dot{y}_0\end{bmatrix} = \begin{bmatrix}\phi_{43} & \phi_{45} \\ \phi_{63} & \phi_{65}\end{bmatrix}^\dagger \begin{bmatrix}\delta\dot{x}_t \\ \delta\dot{z}_t\end{bmatrix} \tag{2.34}$$

This formulation can be easily modified if a correction on x_0 were to be desired. Both methods were in fact used to compute suitable initial conditions.

In order to find $t = \frac{T}{2}$, a shooting method can be adopted: target is t that corresponds to the x-z plane crossing, or $y_t = 0$.

Having a starting guess, which can be recovered by tables or by an analytical guess [42], this initial condition is updated in order to find a suitable initial condition for a repeating orbit. The starting guess is:

$$\begin{bmatrix}x_0 \\ y_0 \\ z_0 \\ \dot{x}_0 \\ \dot{y}_0 \\ \dot{z}_0\end{bmatrix} = \begin{bmatrix}1.124242839945290 \\ 0 \\ 0.187435048916681 \\ 0 \\ -0.223784191244108 \\ 0\end{bmatrix} \tag{2.35}$$

and the refined condition is:

$$\begin{bmatrix} x_0 \\ y_0 \\ z_0 \\ \dot{x}_0 \\ \dot{y}_0 \\ \dot{z}_0 \end{bmatrix} = \begin{bmatrix} 1.124242839945290 \\ 0 \\ 0.182846789055170 \\ 0 \\ -0.225326578364074 \\ 0 \end{bmatrix} \tag{2.36}$$

This initial condition provides a repeating orbit with period T equal to 2.9475τ, which corresponds to 12.81 days, and is represented in figure 2.3. Since the ODE set provides an orbit in normalized quantities, a backward transformation to not-normalized units is required. For the circular case, the characteristic time and length are constant, therefore no deformation is introduced in the orbit shape.

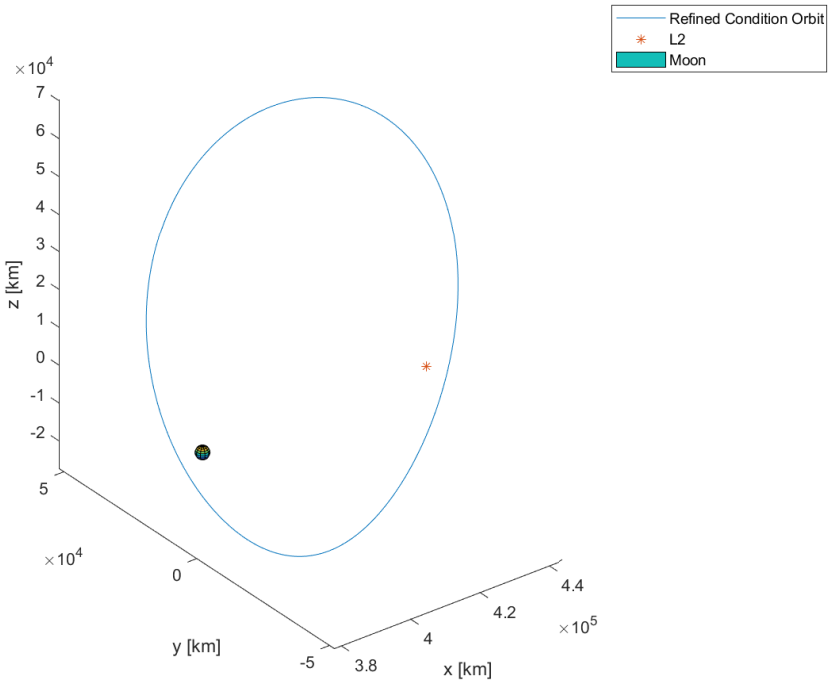

Figure 2.3: Refined periodic orbit

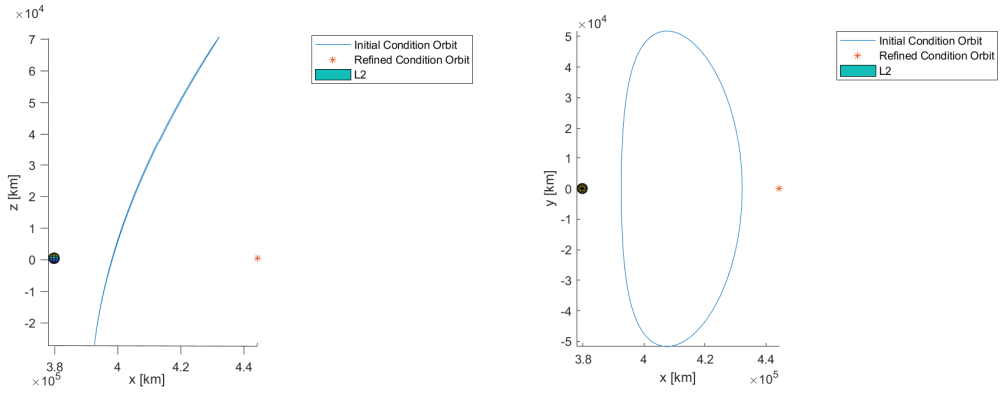

Figure 2.4: Refined periodic orbit in the xz-plane (left) and xy-plane (right)

2.2 Elliptical Restricted 3-Body Problem

The CR3BP is an autonomous model which has an inherent approximation, consisting in the circular orbit of the smaller primary. However, in order to provide a more rigorous model, it is necessary to include the information about eccentricity. For the Earth-Moon system, eccentricity e has a value $e = 0.0549$. The inclusion of this term into the equations of motion mutates the problem into the Elliptical Restricted 3-Body Problem (ER3BP). This new model has significant differences as compared to that of the CR3BP:

- Position of Lagrange points is not constant
- Jacobi Integral is time-dependent
- STM is modified.

In this new model, l^* is no more constant, but it depends on the value of true anomaly θ following the equation:

$$l^* = \frac{a(1-e^2)}{1+ecos\theta} \tag{2.37}$$

Angular velocity is also θ-dependent, as its derivative:

$$n = \frac{(1+ecos\theta)^2}{(1-e^2)e^{\frac{3}{2}}}$$

$$\dot{n} = -2e\frac{sin\theta}{(1-e^2)^{\frac{3}{2}}}$$

2.2.1 Equation of Motion

As carried out for the CR3BP, the position, velocity and acceleration coordinates in rotating frame becomes:

$$\begin{bmatrix}\rho_x\\ \rho_y\\ \rho_z\end{bmatrix} = \begin{bmatrix}x\\ y\\ z\end{bmatrix}$$
$$\begin{bmatrix}\dot{\rho}_x\\ \dot{\rho}_y\\ \dot{\rho}_z\end{bmatrix} = \begin{bmatrix}\dot{x}-ny\\ \dot{y}+nx\\ \dot{z}\end{bmatrix}$$
$$\begin{bmatrix}\ddot{\rho}_x\\ \ddot{\rho}_y\\ \ddot{\rho}_z\end{bmatrix} = \begin{bmatrix}\ddot{x}-2n\dot{y}-\dot{n}y-n^2x\\ \ddot{y}+2n\dot{x}+\dot{n}x-n^2y\\ \ddot{z}\end{bmatrix}$$

Using this formulation, equation of motion becomes:

$$\ddot{x}-2n\dot{y}-\dot{n}y-n^2x = -\frac{(1-\mu)(x+\mu\sigma)}{d^3}-\frac{\mu(x-(1-\mu)\sigma)}{r^3}$$
$$\ddot{y}+2n\dot{x}+\dot{n}x-n^2y = -\frac{(1-\mu)y}{d^3}-\frac{\mu y}{r^3}$$
$$\ddot{z}-\frac{(1-\mu)z}{d^3}-\frac{\mu z}{r^3}$$

where

$$\overrightarrow{d} = (x+\mu\sigma)\hat{X}+y\hat{Y}+z\hat{Z}$$
$$\overrightarrow{r} = (x-(1-\mu)\sigma)\hat{X}+y\hat{Y}+z\hat{Z}$$
$$\sigma = \frac{1-e^2}{1+ecos\theta}$$

The pseudo potential becomes:

$$U = \frac{1}{2}n^2(\dot{x} + \dot{y})^2 + \frac{1-\mu}{d} + \frac{\mu}{r} \tag{2.38}$$

which demonstrates how the Jacobi Integral becomes time-dependent. There exist, however, a different way to define motion in the ER3BP. This different methodology requires the introduction of a new reference: Pulsating-Rotating reference frame.

The Pulsating-Rotating reference frame is able to fix the relative distance between the primaries, in the normalized set of equation of motion, and makes the problem θ-dependent. Therefore, all the quantities of interest (position, velocity, acceleration) are expressed in terms of true anomaly. Following the procedure explained by Szebehely [44] and Ferrari [12], in its PhD thesis, and used by [5][6], equation of motion can be written in this new reference frame as:

$$\begin{aligned} \ddot{x} - 2\dot{y} &= \frac{1}{1 + e cos\theta}\frac{\partial \Omega}{\partial x} \\ \ddot{y} + 2\dot{x} &= \frac{1}{1 + e cos\theta}\frac{\partial \Omega}{\partial y} \\ \ddot{z} + z &= \frac{1}{1 + e cos\theta}\frac{\partial \Omega}{\partial z} \end{aligned}$$

where

$$\Omega = \frac{1}{2}(\dot{x} + \dot{y} + \dot{z})^2 + \frac{1-\mu}{d} + \frac{\mu}{r} \tag{2.39}$$

2.2.2 State Transition Matrix

The overall theory behind the computation of the State Transition Matrix doesn't change, since it is again referred to the evolution of a given state vector along time.

Due to the different state-space representation of the equation of motion, however, there is a slight change in the computation of the **A** matrix, particularly in the

computation of the U_{dd} components. The double partial derivatives become:

$$U_{xx} = \frac{1}{1+ecos\theta}(1 - \frac{1-\mu}{d^3} - \frac{\mu}{r^3} + 3\frac{(1-\mu)(x+\mu\sigma)^2}{d^5} + 3\frac{\mu(x-(1-\mu)\sigma)^2}{r^5})$$

$$U_{yy} = \frac{1}{1+ecos\theta}(1 - \frac{1-\mu}{d^3} - \frac{\mu}{r^3} + 3\frac{(1-\mu)y^2}{d^5} + 3\frac{\mu y^2}{r^5})$$

$$U_{zz} = \frac{1}{1+ecos\theta}(\frac{1-\mu}{d^3} - \frac{\mu}{r^3} + 3\frac{(1-\mu)z^2}{d^5} + 3\frac{\mu z^2}{r^5})$$

$$U_{xy} = U_{yx} = \frac{1}{1+ecos\theta}(3\frac{(1-\mu)(x+\mu\sigma)y}{d^5} + 3\frac{\mu(x-(1-\mu)\sigma)y}{r^5})$$

$$U_{xz} = U_{zx} = \frac{1}{1+ecos\theta}(3\frac{(1-\mu)(x+\mu\sigma)z}{d^5} + 3\frac{\mu(x-(1-\mu)\sigma)z}{r^5})$$

$$U_{yz} = U_{zy} = \frac{1}{1+ecos\theta}(3\frac{(1-\mu)yz}{d^5} + 3\frac{\mu yz}{r^5})$$

2.2.3 Orbit Generation

The initial condition needs to be updated to fit the ellipticity of the model. This section will describe the algorithm that will be followed to generate initial conditions for the ER3BP. The right hand side of the equations of motion is periodic with period 2π. Thus, periodic solutions of the ER3BP must have period T = 2Nπ, N = 1, 2, ...

In the context of the planar ER3BP, Moulton [33] used these considerations and the symmetry properties to formulate the Strong Periodicity Criterion:

- For an orbit to be periodic [in the planar ER3BP] it is sufficient that it has two perpendicular crossing with the x-z plane
- The crossings happen when the two primaries are at an apse

With these considerations, it is no more sufficient to only impose perpendicular crossing as previously done in the CR3BP, because crossing time becomes crucial. Starting from the refined initial condition found in the CR3BP, the variational approach has been adopted to provide refinements to the initial condition. The corrective term $\delta\overrightarrow{x}_0$ has been computed considering the fact that two conditions must be valid.

The adopted procedure is the following:

1. Impose crossing of y-axis at $t = \pi$, computing $\delta\overrightarrow{x}_t = [0, \delta y_t, 0, \delta\dot{x}_t, 0, \delta\dot{z}_t]^T$ and evaluating $\delta\overrightarrow{x}_0 = [\delta x_0, 0, \delta z_0, 0, \delta\dot{y}_0, 0]^T$. Inverse computation becomes easier due to the fact that $\phi(t, t_0)$ can be written as a 3x3 square matrix

2. Impose perpendicular crossing at $t = \pi$, computing $\delta\overrightarrow{x}_t = [0, \delta y_t, 0, \delta\dot{x}_t, 0, \delta\dot{z}_t]^T$ and evaluating $\delta\overrightarrow{x}_0 = [0, 0, \delta z_0, 0, \delta\dot{y}_0, 0]^T$.

3. Repeat point 1-2 until desired orbit becomes periodic and repeating.

This methodology proved to be useful in recovering a suitable initial condition for the ER3BP, that starting from the initial guess of Narula and Biggs [35]:

$$\begin{bmatrix} x_0 \\ y_0 \\ z_0 \\ \dot{x}_0 \\ \dot{y}_0 \\ \dot{z}_0 \end{bmatrix} = \begin{bmatrix} 1.13424283994529 \\ 0 \\ 0.187435048916681 \\ 0 \\ -0.223784191244108 \\ 0 \end{bmatrix} \tag{2.40}$$

has been updated to:

$$\begin{bmatrix} x_0 \\ y_0 \\ z_0 \\ \dot{x}_0 \\ \dot{y}_0 \\ \dot{z}_0 \end{bmatrix} = \begin{bmatrix} 1.149619657045652 \\ 0 \\ 0.165528132267168 \\ 0 \\ -0.251414419543829 \\ 0 \end{bmatrix} \tag{2.41}$$

The obtained orbit is shown in figure 2.5 in normalized units. It can be noted that it's shape is not actually a classical halo around the Moon, like the one provided in the CR3BP section. Also, the same procedure of non-normalization must be performed. In this case, the characteristic length changes in time, therefore a deformation will be introduced. This effect is clear in figure 2.7.

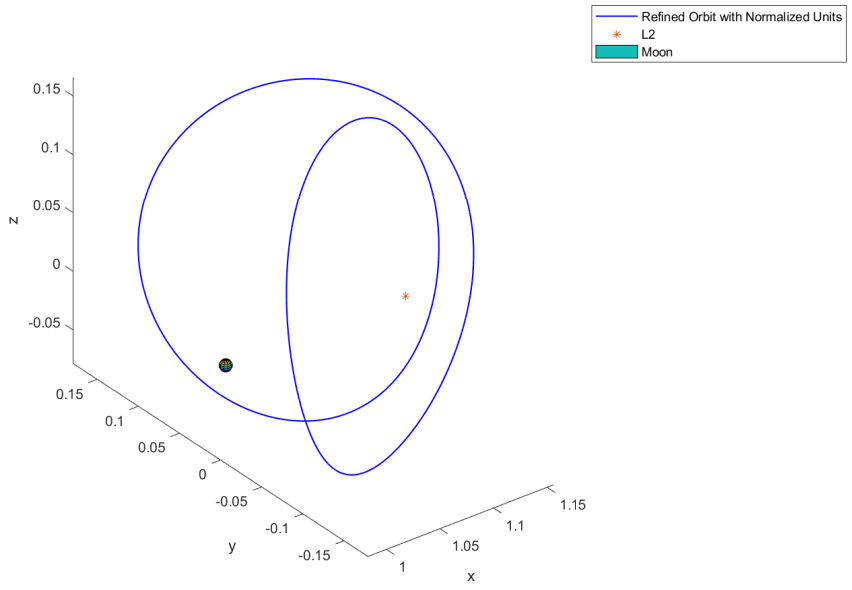

Figure 2.5: Repeating Halo Orbit in the ER3BP, normalized units

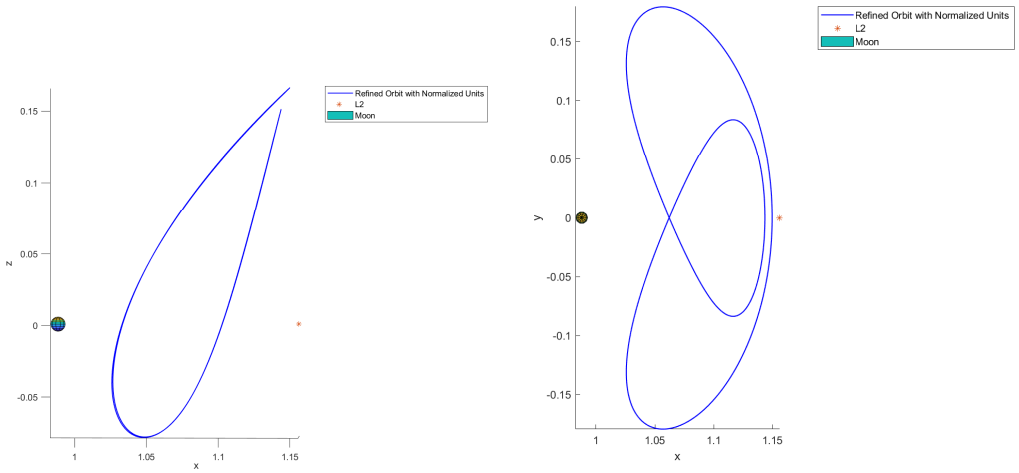

Figure 2.6: Periodic orbit in the xz-plane (left) and xy-plane (right), normalized units

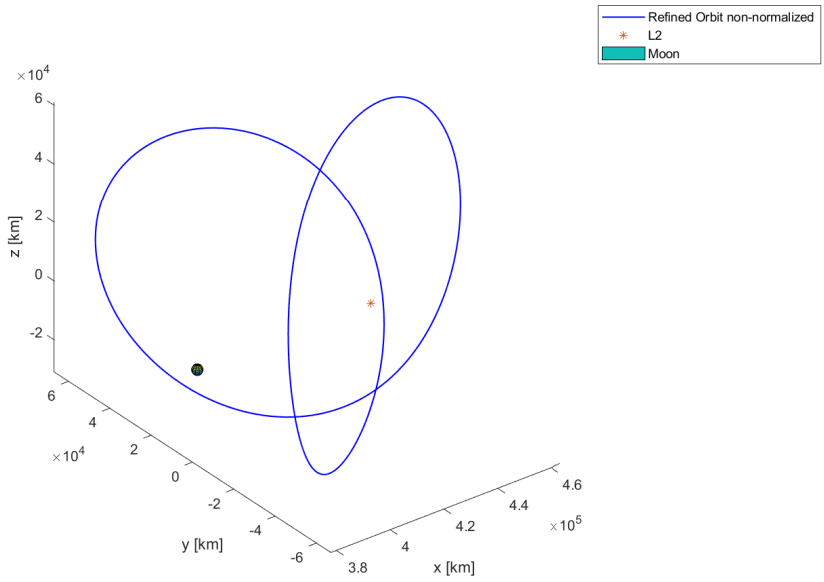

Figure 2.7: Repeating Halo Orbit in the ER3BP

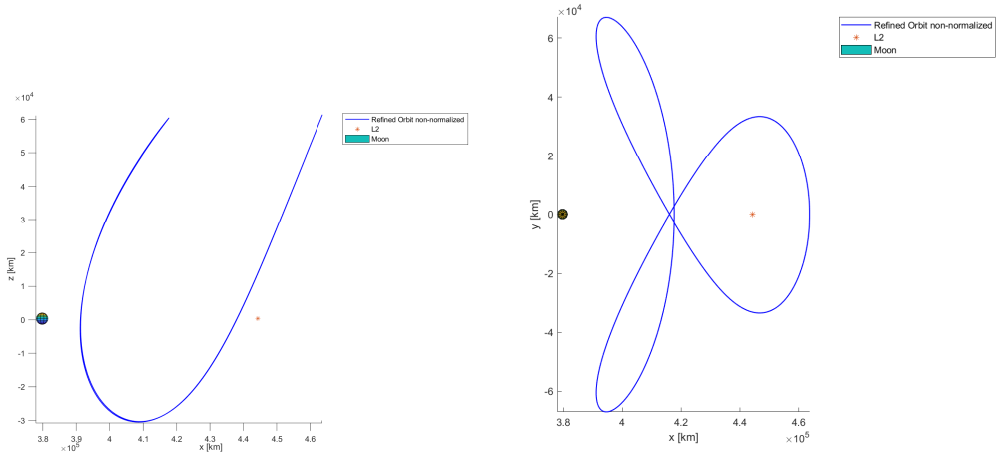

Figure 2.8: Periodic orbit in the xz-plane (left) and xy-plane (right)

It can also be shown that a similar shape can be obtained by a classical halo orbit, as the one of figure 2.3. First, the orbit found in the CR3BP must be updated in order to impose a period of 2π, since this guarantees crossing of the x-z plane when the primaries are at an apse.

Starting from the initial guess:

$$\begin{bmatrix} x_0 \\ y_0 \\ z_0 \\ \dot{x}_0 \\ \dot{y}_0 \\ \dot{z}_0 \end{bmatrix} = \begin{bmatrix} 1.124242839945290 \\ 0 \\ 0.187435048916681 \\ 0 \\ -0.223784191244108 \\ 0 \end{bmatrix} \tag{2.42}$$

and implementing the same procedure, but in the CR3BP work-frame, the initial condition is updated to:

$$\begin{bmatrix} x_0 \\ y_0 \\ z_0 \\ \dot{x}_0 \\ \dot{y}_0 \\ \dot{z}_0 \end{bmatrix} = \begin{bmatrix} 1.126756126623475 \\ 0 \\ 0.184036459910411 \\ 0 \\ -0.201986794155454 \\ 0 \end{bmatrix} \tag{2.43}$$

The new initial condition provides an orbit with period T=π if seen in the CR3BP and it still resembles a classical halo-orbit around the Moon. Two full orbits correspond instead to a time $\tau = 2\pi$.

In the ER3BP, however, the characteristic length varies in time and this effect causes the two perpendicular crossings to happen at different distances from the E-M system barycenter. Orbit apoapsis and periapsis therefore stop coinciding and become two separate points. The orbital period becomes T=2π, which is consistent with the hypothesis of crossing of the x-z plane when the primaries are at an apse. The effect of this transformation is seen in figure 2.9.

This demonstrates that the shape of an orbit also depends on the work-frame in

which it is represented and that a classical halo orbit can deform to a completely different shape.

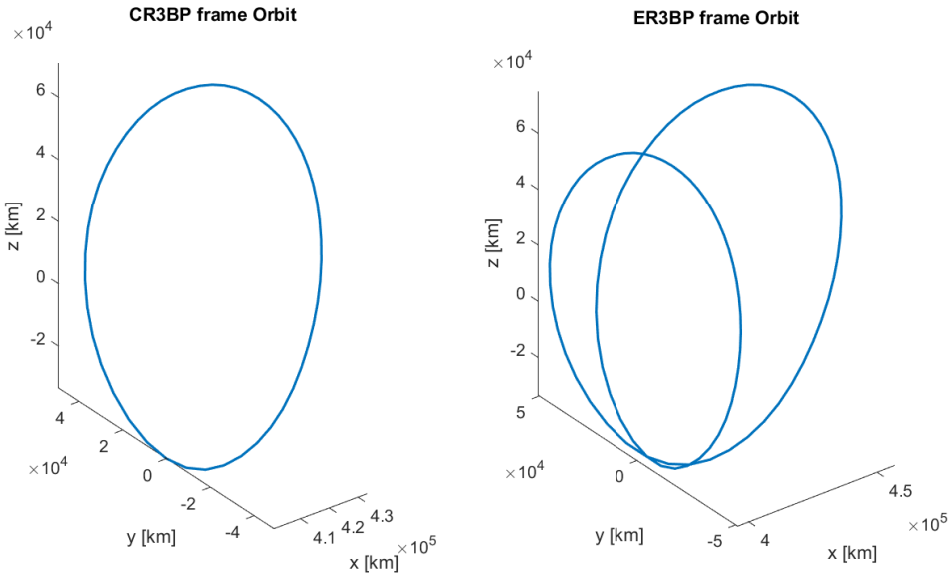

Figure 2.9: Periodic orbit in CR3BP and in ER3BP work-frame

2.3 Reference Computation

Having identified some nominal trajectories, a suitable reference trajectory is necessary in order to compute the reference $\overrightarrow{X}_{ref}$. To this end, various strategies are suggested by Howell [38], Folta [13] to keep the actual trajectory of the spacecraft sufficiently close to the reference path.

As a first approximation, the quasi-periodic orbit that derives from suitable initial conditions can be approximated through a Fourier series, such that:

$$i_{ref} = a_0^i + \sum_{k=1}^{n} (a_k^i cos(k\omega t) + b_k^i sin(k\omega t)) \tag{2.44}$$

Where k represents series order and $i = x_{ref}, y_{ref}, z_{ref}, \dot{x}_{ref}, \dot{y}_{ref}, \dot{z}_{ref}$. t can be intended as τ, in case of CR3BP, or as true anomaly θ, in case of ER3BP.

In order to improve the reference approximation, particularly for the ER3BP case, a different approach has been adopted. Instead of computing the reference through the Fourier series for $\theta = \hat{\theta}$, the equation of motion would be solved, starting from the refined initial condition, from $\theta = \theta_0$ to $\theta = \hat{\theta}$.

The possible drawback that can arise from this methodology is the fact that the initial condition for ER3BP doesn't produce a perfectly repeating orbit, therefore motion, and thus reference, would diverge in time. Moreover, in absence of external disturbances, reference and spacecraft motion would always coincide, thus no control action would be performed and no station-keeping would be possible. Wrapping the solution to 2π mitigates these effect and provides a fixed reference in time, suitable for station-keeping purpose, while removing the approximation that a Fourier series approach would introduce, at the expense of a small discontinuity at t=2π.

Chapter 3

Control Algorithm

This chapter will introduce the station-keeping concepts and methodologies that are adopted to control the Halo orbit. The first control is a simple continuous LQR [35], which is later modified into a discrete, continuous LQR [3]. The next step consists in a further improvement, which allows the realization of an impulsive control, the first element of novelty of the thesis. In order to improve the response of the spacecraft motion, the proportional LQR is augmented with the addition of a derivative element in the control, a second element of novelty. Both strategies are joined together and improved thanks to an act-and-wait strategy [40] and a Schmidt trigger control, based on [31].

The Lagrange points are equilibrium points that, as previously shown, can be found through the use of zero-velocity curves. Unfortunately, only L4 and L5 are stable points, while L1, L2, L3 are unstable equilibrium points. This means that the computation of a periodic orbit is not enough to guarantee asymptotic stability for a spacecraft orbiting close to these points and a proper control algorithm must be implemented to achieve station-keeping. Without this technique, the natural disturbances that a spacecraft undergoes in its orbit would be enough to make its motion divergent.

There have been many strategies explained in literature with respect to station-keeping in the Sun-Earth system [5][6], but fewer studies have considered trajectories

near the Earth-Moon Lagrangian points [13][14][15] as it is more challenging in the Earth-Moon system, due to the larger orbital eccentricity of the secondary.

The unique operational constrains are achieving a controlled orbit with minimum cost in terms of fuel as well as limiting the required control effort. Presently, station-keeping costs of less than 200 m/s per year are desired [13].

3.1 Continuous Control

The goal of the station keeping process is to compute and implement maneuvers to maintain a vehicle within the enclosed region defined by a torus centered at a point along the trajectory, point by point, in time. The simplest way to integrate the station keeping is through a continuous control. The following sequence of steps are adopted to perform the station-keeping:

1. At any given instant, identify weather a station-keeping maneuvers is required
2. If required, compute the magnitude and direction of the control u
3. Optimize the gain in conjunction with the maximum thrust available from the thrusters
4. Implement tracking and sensor errors to the problem

Spacecraft station-keeping on Libration Point Orbits can be categorized into two types: impulsive thrust station-keeping (usually chemical) where the controls are discontinuous and continuous, low-thrust, station-keeping (such as solar electric propulsion or solar sail spacecraft). Xin [50] used a sub-optimal control technique (the θ - D technique) to complete the mission of multiple spacecraft formation flying in deep space about the L2 point. Marchand and Howell [32] employed feedback linearization for formation flight in the vicinity of Lagrangian points. Bai and Junkins[2] proposed a modified Chebyshev-Picard integration method for station-keeping of L2 Halo orbits in the Earth-Moon system. Karimi [52] solved the problem of Halo orbit

control using optimal control theory and the extension of the active disturbance rejection technique to counter the external disturbances in the unstable orbit near the co-linear points. Narula and Biggs [35] compared different approaches to a simple LQR scheme for continuous control with partial thrust failures. Biggs et al. [6] developed a time-delayed feedback controller for the case of solar sail propulsion, which checked the error after one orbit thanks to a state transition matrix exploitation. Bai et al. [1] developed an adaptive control with active disturbances rejection, applied to a quaternion attitude tracking problem.

Having identified the initial conditions and the reference trajectory, the aim is now to have a control algorithm for such an unstable periodic orbit for all the three axis of the spacecraft. In order to optimize the use of propellant, an LQR control is developed considering the thruster model for the actuation of spacecraft as continuous. In some cases the control is also highly nonlinear such as in the case of a solar sail [5][6] and a traditional approach consists in firstly linearize the nonlinear system of the form:

$$\ddot{\mathbf{X}}_1 = g(\dot{\mathbf{X}}_1, \mathbf{X}_1, u) + d \tag{3.1}$$

where $\mathbf{X}_1$, $\dot{\mathbf{X}}_1$, $\ddot{\mathbf{X}}_1$, u, d are respectively the position, velocity, acceleration, control and disturbance vectors and g is a known non-linear function. Expanding the state space, the system can be written in the form:

$$\dot{X} = f(X, u) + d \tag{3.2}$$

where $X = [X_1, \dot{X}_1]$ is the state. Linearizing the nonlinear equations by defining:

$$\Delta\overrightarrow{X} = \overrightarrow{X}_{ref} - X \tag{3.3}$$

where $\overrightarrow{X}_{ref}$ denotes the reference trajectory, yields to the linear system:

$$\Delta\dot{\overrightarrow{X}} = \mathbf{A}(t)\Delta\overrightarrow{X} + \mathbf{B}u \tag{3.4}$$

which is a linear time-varying system, with:

$$A(t) = \begin{bmatrix} \mathbf{0}_{3x3} & \mathbf{I}_{3x3} \\ \mathbf{U}_{dd} & 2\mathbf{\Omega} \end{bmatrix} \tag{3.5}$$

$$\mathbf{B} = \begin{bmatrix} 0 & 0 & 0 \\ 0 & 0 & 0 \\ 0 & 0 & 0 \\ 1 & 0 & 0 \\ 0 & 1 & 0 \\ 0 & 0 & 1 \end{bmatrix} \tag{3.6}$$

and u is the control vector. It was also found that A(t) does not change much along the reference trajectory, thus in order to have a simplified control design, the following linear time invariant model can also be assumed as:

$$\Delta\dot{\overrightarrow{X}} = \mathbf{A}\Delta\overrightarrow{X} + \mathbf{B}u \tag{3.7}$$

where

$$\mathbf{A} = \begin{bmatrix} \mathbf{0}_{3x3} & \mathbf{I}_{3x3} \\ \mathbf{U}_{dd} & 2\mathbf{\Omega} \end{bmatrix}_{\overrightarrow{X}_0} \tag{3.8}$$

$\overrightarrow{X}_0$ is a suitable point belonging to the reference trajectory, such as the initial point of the trajectory. A simple controller is given by:

$$u = -\mathbf{K}\Delta\overrightarrow{X} \tag{3.9}$$

where the gain matrix $\mathbf{K}$ can be solved through the minimization of the cost function:

$$J = \int_{t_0}^{t} [\Delta\overrightarrow{X}^T\mathbf{Q}\Delta\overrightarrow{X} + u^T\mathbf{R}u]dt \tag{3.10}$$

The solution to the minimization can be obtained using the method of Lagrange multiplier and leads to the following Riccati equation:

$$SA + A^T S - SBR^{-1}B^T S + Q = 0 \tag{3.11}$$

where Q, R are two weights that quantify the relative cost of each state and control in the cost function. The values for $\mathbf{Q}$,$\mathbf{R}$ has been selected from [35] and then manually adjusted and are listed in table 3.1

Matrix	**Value**
Q	diag(100,100,100,1,1,1)
R	diag(0.04,0.04,0.04)

Table 3.1: Weight matrices

Having solved the equation for S, the gain matrix can be obtained as:

$$\mathbf{K} = R^{-1}B^T S(t) \tag{3.12}$$

Having found the value of control action u, it can be plugged in the equation of motion. In case of ER3BP, it becomes:

$$\ddot{x} - 2\dot{y} = \frac{1}{1 + e cos\theta}(\frac{\partial \Omega}{\partial x} + u_x)$$
$$\ddot{y} + 2\dot{x} = \frac{1}{1 + e cos\theta}(\frac{\partial \Omega}{\partial y} + u_y)$$
$$\ddot{z} + z = \frac{1}{1 + e cos\theta}(\frac{\partial \Omega}{\partial z} + u_z)$$

3.2 Discrete Control

A different methodology would be to implement a discrete LQR, as explained in [3]. The actuation is performed using thrusters which provide impulsive thrust with a sampling interval Ts and a duration d, therefore the control vector u is defined as follows:

$$u(t) = \begin{cases} u_k/d & \text{if } t_k \leq t \leq t_k + d \\ 0 & \text{if } t_k + d < t \leq t_k + T_s \end{cases}$$

In the notation, T_s represents the sampling interval, d is the thrust duration, k represents the sampling index and $u_k = [\Delta v_x, \Delta v_y, \Delta v_z]^T$ is the control signal (in velocity units) provided by a discrete-time controller.

In the limit case where $d \to 0$ and $T_s > d$, the control signal becomes impulsive:

$$u(t) = u_k \delta(t - t_k), tk \leq t \leq t_{k+1}, k = 0, 1, 2, ... \tag{3.13}$$

where $\delta(t - t_k)$ is the Dirac delta function defined as:

$$\delta(t - t_k) = 0, t \neq t_k \tag{3.14}$$

and

$$\int_{-\infty}^{+\infty} \delta\tau d\tau = 1 \tag{3.15}$$

If d is selected such that $d = T_s$, the control becomes $u(t) = u_k/d$ for $t_k \leq t \leq t_{k+1}$, which is constant between sampling instants. This is a common assumption in discrete-time control.

The computation of the control *u(t)* is similar as in the continuous control case, but it is done considering discrete quantities. Since the gain matrix $\mathbf{K}$ is a matrix that allows the transformation from an error to an acceleration, the equation used to compute u_k becomes:

$$u_k = -\mathbf{K}\Delta X_k T_s \tag{3.16}$$

where ΔX_k is the discretized error state. In this way, when computing the control effort *u(t)* as:

$$u(t) = \begin{cases} u_k/d & \text{if } t_k \leq t \leq t_k + d \\ 0 & \text{if } t_k + d < t \leq t_k + T_s \end{cases}$$

no error is made, as u_k is in the form of a velocity. It represents the impulse required for the particular sample interval k.

The difference with a continuous control lies in the fact that the discrete control only updates the error state at the beginning of a new sampling interval, then it remains constant for its duration , while the continuous control is continuously updating the error and compensating accordingly. The two controls provide the same value only when the discrete controller updates the error state, afterwards they diverge. This implies that the discrete controller provides an action that relies on not-trustworthy information, and this behaviour becomes more intense as time approaches the end of the sampling interval. It is therefore good practice to reduce the duration of the sampling interval T_s, or to develop a control capable of providing the required impulse in a short amount of time, closer to the beginning of the sampling interval, where the information is more up-to-date.

The possible drawbacks that can be encountered are an increased computational effort in case of T_s reduction, therefore the choice of this value must be studied in order to find a suitable compromise between control performance and computational performance.

The linear time invariant model is however not discretized and it remains continuous. Only the control is discretized through this procedure, implementing a zero-order holder in the Simulink environment of the simulation.

3.3 Impulsive Control Hypothesis

A drawback of a continuous control is the fact that thrust level must be adapted to match the required control effort, which may reach low values. These values might be out of specs for the chosen thruster. Moreover, this kind of control requires the thruster to be always on, therefore leaving not enough time for an attitude correction maneuver to change spacecraft pointing to the required direction.

A possible solution would be to concentrate the nominal control into smaller windows of time, while simultaneously increasing the control effort in order to maintain

the same nominal required impulse. The idea behind this implementation lies in the fact that the simulation, while trying to simulate a continuous system, computes the required control point by point, which are separated by a certain amount of time. Linearizing the control between two points, the area subtended is equal to the impulse that the thruster must provide in the identified nominal interval.

This procedure would be implemented in a post-processing phase, after the completion of the orbital dynamics simulation and would transform the continuous control into an impulsive control.

If the thrust level of the engine is known, together with spacecraft mass, the nominal acceleration a that the thruster can provide is known. Since the required impulse i along x,y,z can be computed, it is straightforward to compute the new interval length τ and the new control action that would provide the same impulse as the one from the nominal interval t_{nom}:

$$\begin{cases} \tau = \frac{1}{a}\sqrt{i_x^2 + i_y^2 + i_z^2} \\ u_x = i_x/\tau \\ u_y = i_y/\tau \\ u_z = i_z/\tau \end{cases}$$

Visually, the effect is seen in figure 3.1.

This methodology does not solve the problem related to a control action higher than the maximum allowable by the thruster. However, a saturation algorithm could be implemented in the simulation that would limit the control output. Of course, it would require the upper limit of the net acceleration provided by the spacecraft, a quantity that must also undergo normalization with a time-varying characteristic length.

It is possible that for some intervals the value of τ might be below the minimum activation interval for the thruster. In these cases, a strong approximation has been introduced, which consists in neglecting those intervals. Due to the consequently small required impulse, the error introduced by this decision should be low. A study must be performed to verify if it actually negligible or not.

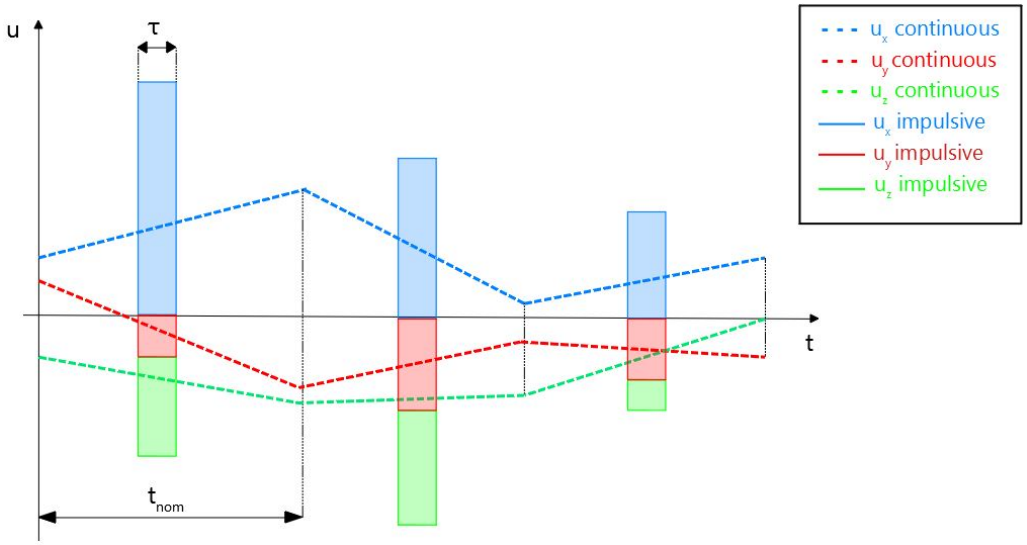

Figure 3.1: Continuous control to impulsive control

A more severe problem lies in the fact that this procedure is performed outside of the simulation work-frame, therefore it is mandatory to simulate again the orbital dynamics with the new control history, to validate if spacecraft motion is still controlled. The difficulty in this task is given by the computational effort required by this validation procedure. The time resolution should be selected such that it would be able to identify the smallest interval τ available for the thruster, therefore in the order of the hundredth of a second for a ordinary chemical thruster with minimum impulse time of 0.1s. For a time-span of one orbit, 27.3 days, the simulation would be composed of 235 million time cells, where each one would store the information related to time (scalar), state (length-6 vector), control (length-3 vector), error (length-6 vector) in a 64-bit format. The total size of simulation result would be in the order of tens of Gigabytes, and it would require a considerable amount of time to complete.

Due to these drawbacks, this methodology has not been chosen as a tool to obtain an impulsive control from the continuous one.

3.4 Impulsive Discrete Control

The problem found in the continuous control is that an attitude correction maneuver is required to point the spacecraft in the correct direction. When the control is active, it leaves no time for attitude adjustment, which can't be simply assumed as instantaneous. It is therefore mandatory that some time between two consecutive control actions must be allocated to a slew maneuver to change the attitude. For this reason, the continuous control won't be further analyzed in this chapter, and the search for a suitable control algorithm will solely focus on the discrete LQR. It too must posses the ability to guarantee time between following sample intervals, in order to complete the attitude adjustment required for pointing the spacecraft in the appropriate control direction.

A possible solution consists in defining the value of d as a fraction of the value selected for T_s, in order to partition a sampling interval between a control phase and a waiting phase, which is used to properly point the spacecraft to the desired direction. The magnitude of the control must however take into account this change, and must increase its value in order to compensate for the shorter control window, since the impulse in the sampling interval must remain constant. It may happen that the thrust obtained in this way is higher than the maximum allowable thrust, therefore a saturation algorithm is mandatory to solve this possibility.

The discrete control can be written as:

$$u(t) = -\mathbf{K}\Delta\overrightarrow{X}g(t)\frac{T_s}{d} \tag{3.17}$$

and

$$g(t) = \begin{cases} 1 & \text{if } t_k \leq t \leq t_k + d \\ 0 & \text{if } t_k + d < t \leq t_k + T_s \end{cases}$$

Two possible strategies can be adopted:

1. The first part of the sampling interval is dedicated to the control

2. The second part of the sampling interval is dedicated to the control

Selecting 1), the control equation doesn't change. This methodology also allows the control to act in a time region closer to the beginning of the sampling interval, which, as previously stated, allows the control to rely on updated information about the error state. There is however a problem: the information on the required attitude for the next interval can't be recovered, since the current sampling interval hasn't finished yet. This means that the control developed by the algorithm can't directly be feed-forwarded to the spacecraft, but must be first completely simulated. This control history is however an approximation of the real space environment that is affecting the spacecraft, therefore the control algorithm should be continuously run to develop a certain control history, updated for a certain time length, then feed-forwarded to the spacecraft as a set of commands that would become less reliable in time.

This problem can be mitigated selecting 2), since the control happens in the later part of the sampling interval and therefore the first part of the interval could be used to point the spacecraft to the desired direction. However, the control would happen in the second part of the sampling interval, which is the worst choice due to the aforementioned updating problem. With this methodology, the control equation would become:

$$u(t) = -\mathbf{K}\Delta\overrightarrow{X}g(t)\frac{T_s}{d} \tag{3.18}$$

and

$$g(t) = \begin{cases} 0 & \text{if } t_k \leq t \leq t_k + (T_s - d) \\ 1 & \text{if } t_k + (T_s - d) < t \leq t_k + T_s \end{cases}$$

A hybrid solution could in theory mitigate both problems. A first, short part of the sampling interval can be dedicated to attitude adjustment, followed immediately by the control itself. The last part of the sampling interval would then be left free, for maintenance or scientific purposes. A control of this kind can be represented as:

$$u(t) = -\mathbf{K}\Delta\overrightarrow{X}g(t)\frac{T_s}{d} \tag{3.19}$$

and

$$g(t) = \begin{cases} 0 & \text{if } t_k \leq t < t_k + t_w \\ 1 & \text{if } t_k + t_w \leq t \leq t_k + t_w + d \\ 0 & \text{if } t_k + t_w + d < t \leq t_k + T_s \end{cases}$$

where t_w represents the amount of time dedicated to attitude adjustment. This notation can be also used for 1) and 2). Choosing $t_w = 0$, the equation becomes the one used for 1), while setting $t_w = T_s - d$ provides the equation used for 2).

The possibility of a saturation algorithm must be accounted for, in case of high required thrust, together with the possibility of reducing the value assigned to d on an interval level, which must be considered in case of small required thrust, particularly in the case of chemical thrusters. On the other hand, it may be necessary to increase the value of d, up to the maximum allowable $d = T_s - t_w$. This could prove useful for electric thrusters, given their low thrust level, in order to delay the saturation algorithm as long as possible. Visually, the control would be active following figure 3.2, where the mechanism of changing d is shown, together with some cases. The black dashed line represents the nominal, discrete control, while the blue columns represent the control after the d-changing mechanism and the implementation of maximum and minimum thrust. This distinction is useful in case of throttleable, electric thruster. For a chemical thruster, therefore with a fixed thrust level, the two values merge together within a single value: the nominal thrust.

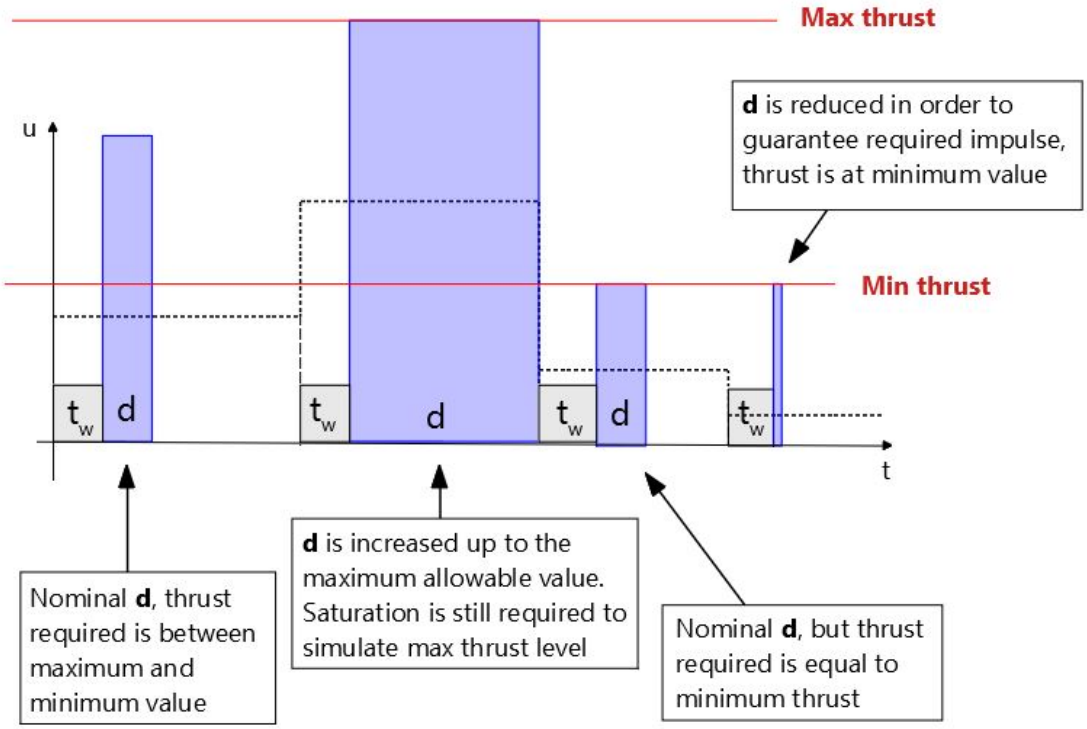

Figure 3.2: Discrete control and some worthy cases

This diagram is valid when the control is in the acting phase. When instead the control is purposely waiting, the action is set to zero.

The complete Simulink algorithm is represented in figure 3.3. The control block collects the adopted methodology for the impulsive discrete transformation of the nominal control coming from the LQR and it can be augmented with the introduction of the act-and-wait and Schmidt trigger strategies.

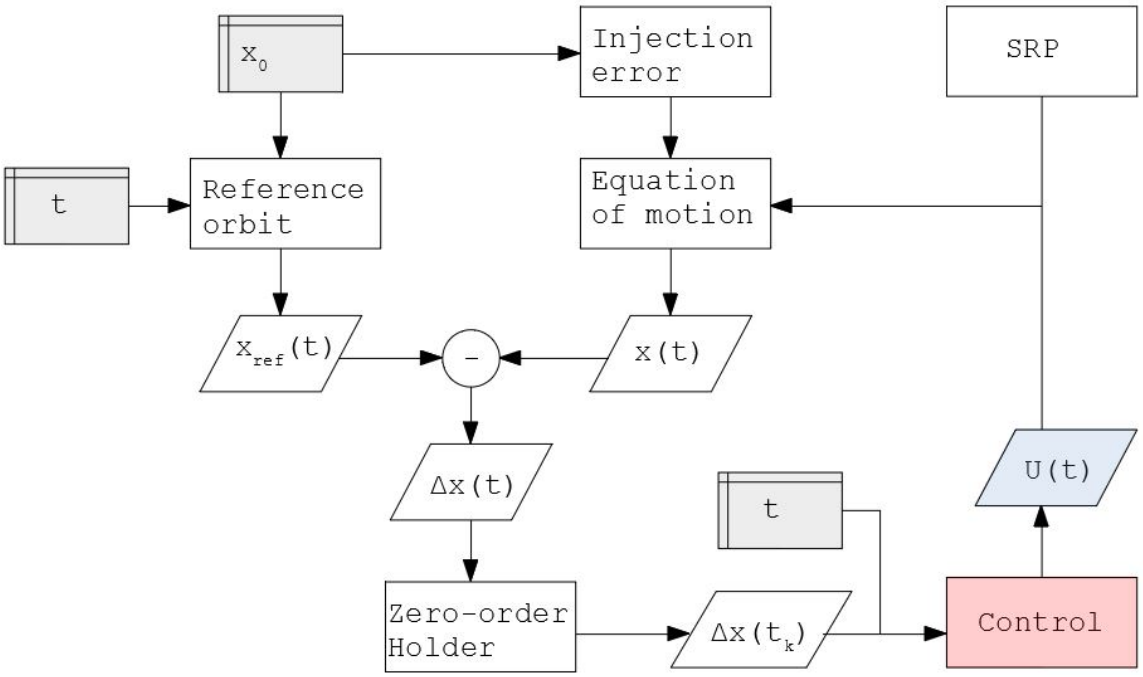

Figure 3.3: Simulink algorithm

3.5 Proportional Derivative Control

The obtained control can be improved by introducing a derivative component within its equation. The introduction of this component can improve the oscillating behaviour of the error state when it is brought to zero from high values:

$$u = -\mathbf{K}\Delta\overrightarrow{X} - k_d\mathbf{K}\mathbf{A}\Delta\overrightarrow{X} \tag{3.20}$$

The term $\mathbf{A}\Delta\overrightarrow{X}$ represents the derivative of the error state and k_d is a parameter to tune the effect of the derivative part of the control.

The idea of this kind of control is based on the fact that, together with the error state, also the velocity at which this state is changing must be considered.

3.6 Act and Wait Algorithm

Depending on the choice of T_s, d, t_w, not enough time can be allocated to scientific purpose, therefore an act-and-wait strategy can be superimposed to allocate long periods of time to this task. This control algorithm would purposely deactivate the control for a certain amount of time, after which it would re-activate it to perform station-keeping maneuvers. A scientific mission would in fact require precise pointing along a specific vector for a suitably long time span. A continuous control could never achieve this task, while the discrete control can partially mitigate achieve this objective by reducing the vale of d. However, only a portion of the sampling interval T_s can be dedicated to the scientific mission, which may not be enough.

Moreover, the position and velocity error are limited within a tiny bound of $\pm$1km and $\pm$5mm/s. These numbers comes from the "Results" section. If these errors would be allowed to slowly increase, thanks to an act-and-wait control type, more time would be left that could be dedicated to a scientific mission. Of course, the period of time where the control loop is off must be carefully chosen, otherwise, at the activation of the control, the effort may reach too high values or, worse, the orbit might start to diverge.

Also, the values of the position and velocity errors can be misinterpreted for a tracking error, which a control algorithm should try to not compensate. Therefore, trying to increase their values before applying any correction is mandatory.

Following the same notation used in [40], a control of this kind can be represented, in a continuous work frame, as:

$$u(t) = -(\mathbf{K}\Delta\overrightarrow{X} - k_p\mathbf{K}\mathbf{A}\Delta\overrightarrow{X})g(t) \tag{3.21}$$

where

$$g(t) = \begin{cases} 1 & \text{if } 0 \leq \text{mod}(t, t_c) \leq t_a \\ 0 & \text{if } t_a < \text{mod}(t, t_c) \leq t_a + t_p \end{cases}$$

The values for t_a and t_p represent the amount of time dedicated to the acting and waiting phases (a pause for the algorithm), respectively, and the condition $t_a + t_p = t_c$

must be satisfied. t_a and t_c can be manually chosen in order to allocate more time to the control or to the scientific mission. t_c, the total cycle duration, affects how many act-and-wait cycles are present in one orbit. Since normalized time is represented in such a way that one full orbit is equal to 2π, the portions of orbit where the control is active can be represented as shown in figure 3.4. Here, two different cycle durations t_c are shown, with a possible t_a. The portion of time, and thus orbit, between t_c and t_a is equal to t_p. On the left, t_c equal to π is selected, while on the right t_c has been chosen equal to 2π. Ideally, if also t_a is doubled from the left case to the right case, an equal amount of time is dedicated to the scientific mission, although it is split into two intervals for the left one. This case should also provide less drift for the spacecraft, and consequently less fuel consumption, because the correcting maneuvers happen more frequently. As noted in [17], the immediate correction of an error is preferable to a delayed correction, due to the fact that an error induces forces that, as time passes, increase said error.

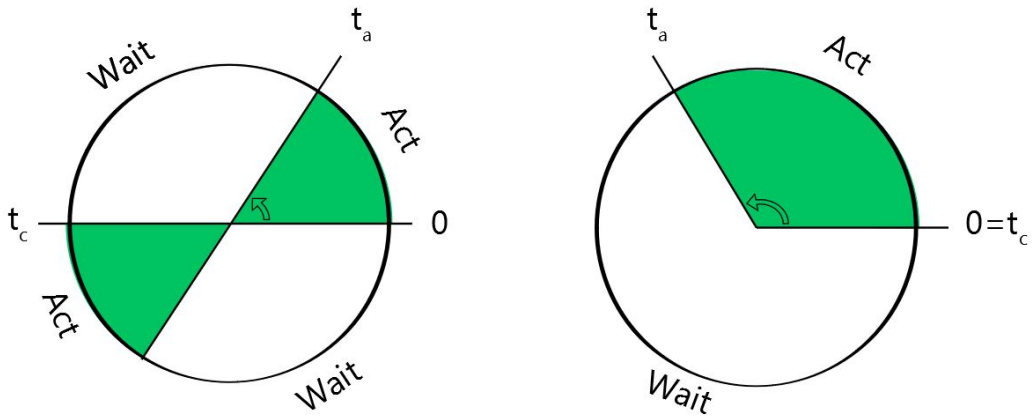

Figure 3.4: Two possible configurations for the act-and-wait control

It is important to select a suitable value for t_a. A small one may not allow enough time to properly control the spacecraft motion, especially in presence of disturbances, therefore making its orbit diverge in time, while a higher value, which can mitigate this problem, may hinder the scientific mission time. On the other hand,

this kind of control allows a precise schedule of time between a station-keeping phase and a scientific one. The complete control block for the act-and-wait algorithm is represented in figure 3.6.

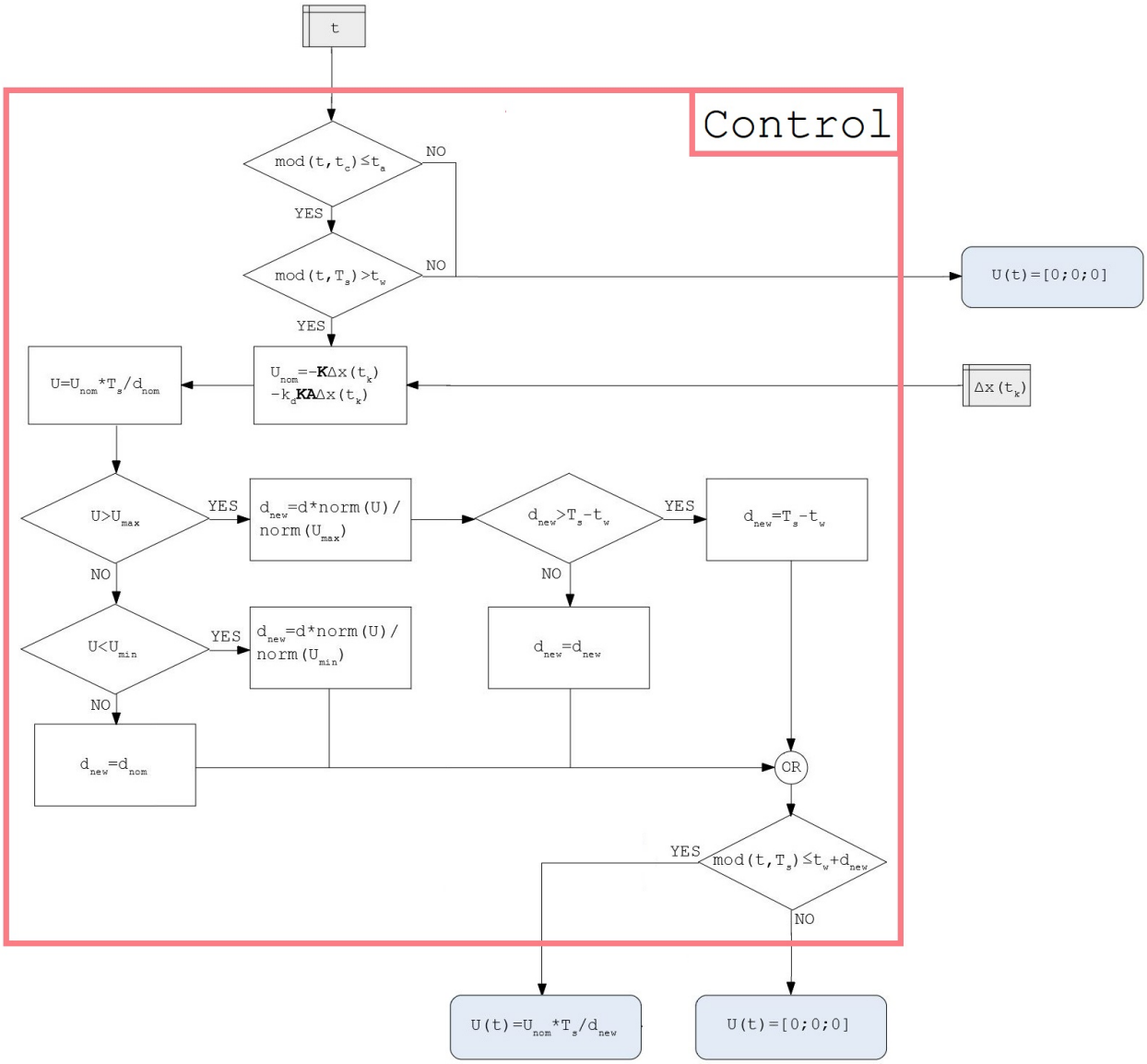

Figure 3.5: Control block detail

3.7 Schmitt Trigger Control

In electronics, a Schmitt trigger is a comparator circuit with hysteresis implemented by applying positive feedback to the non-inverting input of a comparator or differential amplifier [49]. It is an active circuit which converts an analog input signal to a digital output signal. The circuit is named a "trigger" because the output retains its value until the input changes sufficiently to trigger a change. In the non-inverting configuration, when the input is higher than a chosen threshold, the output is high. When the input is below a lower chosen threshold the output is low, and when the input is between the two levels the output retains its value.

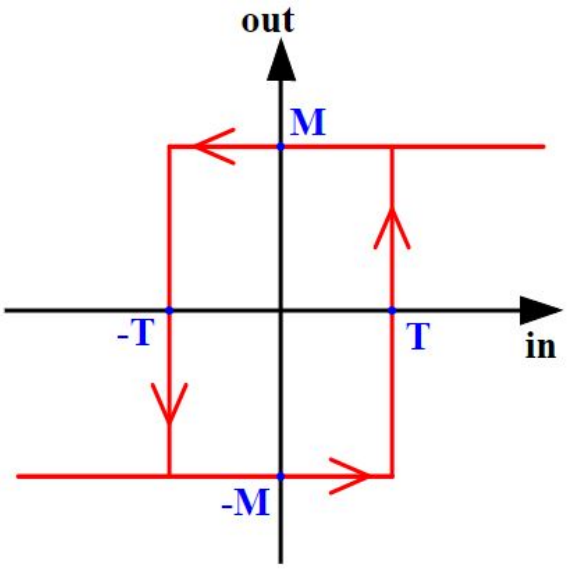

Figure 3.6: Schmitt Trigger transfer function. T - input, M - output

The implementation of a Schmitt trigger allows the introduction of a control that, based on the error state as usual to compute the control action, uses the same state as trigger to decide whether a station-keeping maneuver is required or not. If the error state is above a certain upper threshold, the control is active and tries to bring the error down to a certain lower threshold. On the other end, when the error state is below the upper threshold, no control is active. This idea follows the same principle

introduced with the act-and-wait algorithm, that is to improve the time window available for scientific purpose by letting the position and velocity error increase up to a certain level. Proper bound selection is mandatory to tune the activation and deactivation of the control, which, in a continuous work frame, can be now written as:

$$u(t) = -(\mathbf{K}\Delta\overrightarrow{X} - k_p\mathbf{K}\mathbf{A}\Delta\overrightarrow{X})g(t) \tag{3.22}$$

where $g(t)$ is the Schmitt trigger output, which can assume the limited values of 0 (no control), 1 (control). The output of the trigger depends on the choice of the upper and lower bounds of the trigger, ub and lb. The activation and deactivation of the control follows:

$$\begin{cases} \text{activation:} & |e_p + ke_v| > ub \\ \text{deactivation:} & |e_p + ke_v| < lb \end{cases}$$

e_p and e_v represent the position and velocity error, recovered by the error state $\Delta\overrightarrow{X}$, and k is a weight parameter. The schmitt trigger control logic allows a spacecraft to remain confined within a certain station-keeping box, similar to the work done by Liu et al. [31]. In this case, however, the box also includes the velocity error information, together with the position error.

The main difference with the act-and-wait algorithm is based on the fact that the activation is not based on time, following a predetermined cycle, but based on the error state. This means that no precise schedule can be obtained, due to the fact that the error depends on many possible disturbances that the simulated model doesn't include, therefore the length of time available for scientific mission is hard to predict. On the other hand, no tuning on activation time is required, which is mandatory for the act-and-wait algorithm and critical for the stability of the station-keeping, because the control is solely based on the error state.

The Schmitt trigger can be tuned to work on the position and velocity error or to work independently on the three axis. In this last case, if an axis doesn't require control it is mandatory to redistribute all the available thrust on the two remaining

axis, only. Both cases will be tested.

In case of Schmitt trigger, both the Simulink model and the control algorithm are subjected to changes, which can be seen in figure 3.7 and 3.8. Most notably, the Simulink model requires the introduction of a memory block which stores the information of the control state at the previous step. This block is used to determine if a station keeping maneuver is required, when the error is in the region between the upper and lower bound.

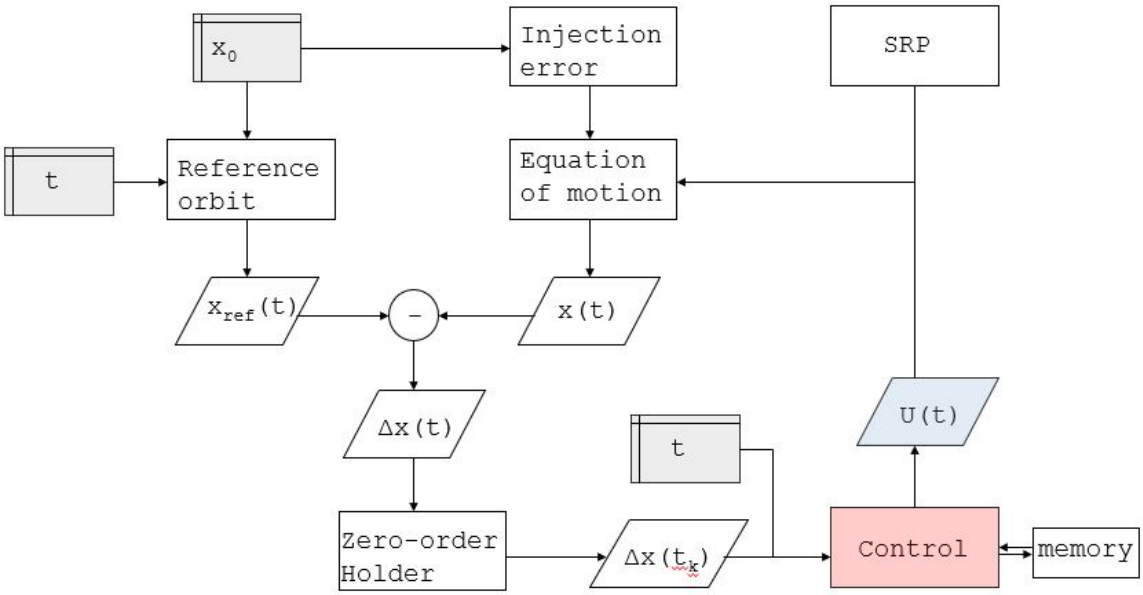

Figure 3.7: Simulink algorithm for Schmitt trigger

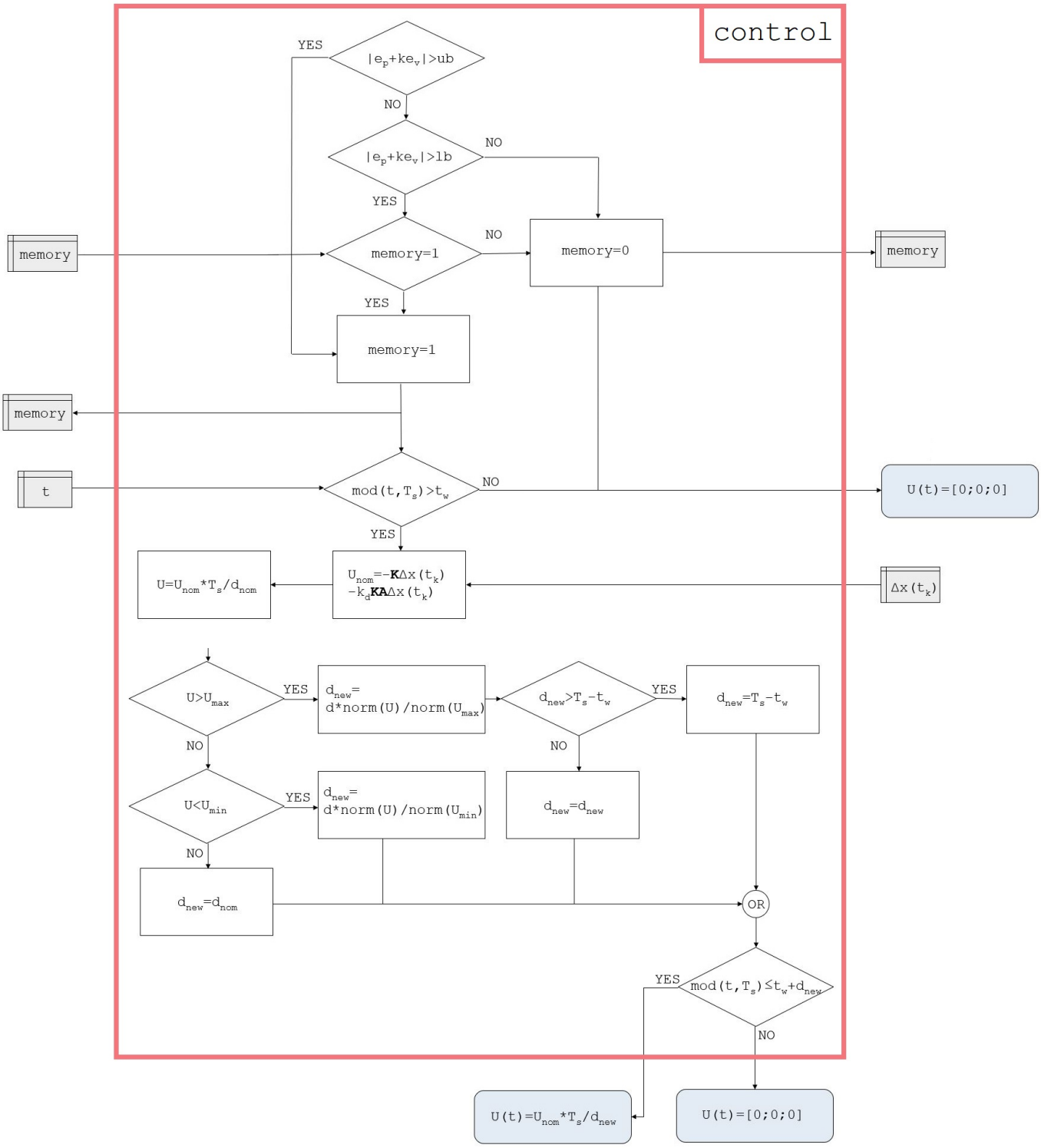

Figure 3.8: Control block detail for Schmitt trigger

3.8 Discarded Ideas

Different control techniques where considered and tested during the thesis project.

Among them, one idea was to use the control itself to drive the spacecraft to a better trajectory than the one computed. The gain matrix $\mathbf{K}$ was slowly reduced until orbital motion started to diverge. Right before diverging, motion was still controlled, but it created a different trajectory than the one provided. This new trajectory was then approximated through a Fourier series and then used as a new reference, with the nominal gain $\mathbf{K}$. Unfortunately, this new reference always performed worse than the nominal one. This behaviour must be due to the inner instability of the L2 point. It is therefore improbable that the reduced control effort could move a spacecraft on a more stable, and thus efficient, orbit. This technique could however work on a L4 or L5 Halo orbit, due to the stability of the two Lagrange points.

A different idea was to use a spherical control, where the control action would maintain a constant mean absolute value, thus suitable for a chemical thruster. The only parameters that would change where two control angles, a horizontal and vertical angle, that would provide the control direction, starting from a suitable, initial vector. This initial vector was obtained after an averaging process of the required control effort with the proportional LQR. Then, in a new simulation, the two control parameters where obtained at each step from a linearization procedure. The control wasn't able to provide a stable station-keeping, even when increasing the control magnitude and the control gain. This behaviour could be due to the linearization procedure, especially when the required control angles are far from the initial vector.

Chapter 4

Simulation Results

In this chapter the results of the various simulations and tests will be shown.

Starting from a comparison between the periodic orbit computed in the CR3BP and the one from the ER3BP, thanks to the refined initial conditions found in chapter 1, the analysis will also test the difference between the Fourier series approximated reference trajectory and the one where the reference comes from the dynamic model.

Later, the first results from the continuous control model will be shown, and then the analysis will focus on the discrete LQR control, introducing all the different strategies previously stated in Chapter 2.

The analysis will be divided between chemical thrusters and electric propulsion.

Before the results are shown, it is necessary to better explain the simulation environment adopted, where the simulation parameters and disturbances are explained. It is also introduced the methodology to assess the performance of the different control strategies, together with the two chosen thrusters data-sheets.

4.1 Simulation Environment

The orbital dynamic scheme is simulated in the Simulink environment, solving the problem through ODE113 scheme, thanks to its higher performance when tolerances are small with respect to ODE45: the relative and absolute tolerances are in fact

set at 10^{-12}. In order to increase the fidelity of the model, some adjustments and additions are introduced.

4.1.1 Solar Radiation Pressure

A spacecraft orbiting close to the L2 Lagrange point is subjected to disturbances that can slowly alter its motion. The task of compensation is entrusted to the control algorithm. The most relevant sources of disturbance come from Solar Radiation Pressure (SRP), Moon non-homogeneous gravity and gravitational influence of other massive bodies, in this case the Sun. Among these, SRP only is taken into account, due to its greater magnitude. The expression to compute its acceleration is given by:

$$\overrightarrow{a}_{SRP} = -\frac{\rho_{SRP} C_r A}{m} \frac{\overrightarrow{r}_{\odot} - \overrightarrow{r}_{S/C}}{|\overrightarrow{r}_{\odot} - \overrightarrow{r}_{S/C}|} \tag{4.1}$$

where ρ_{SRP} is the pressure exerted by the Sun, C_r is the reflection coefficient of the material, A is spacecraft area, normal to the direction of incoming light, m is its mass, $\overrightarrow{r}_{\odot}$ is the position vector of the Sun with respect to system barycenter and $\overrightarrow{r}_{S/C}$ is spacecraft position.

The resulting acceleration, however, must be integrated in the equation of motion in the Pulsating-Rotating reference frame, therefore both $\overrightarrow{r}_{\odot}$ and $\overrightarrow{r}_{S/C}$ must be computed in a Rotating reference frame. $\overrightarrow{r}_{S/C}$ is directly obtained in this frame from the equation of motion, but $\overrightarrow{r}_{\odot}$ is the result of a rotation of angle θ along the z-axis applied to the Sun-inertial position $\overrightarrow{r}^{I}_{\odot}$, which can be computed as:

$$\overrightarrow{r}^{I}_{\odot} = r_{\odot} \begin{bmatrix} \cos(n_{\odot} t) \\ \sin(n_{\odot} t)\cos\epsilon \\ \sin(n_{\odot} t)\sin\epsilon \end{bmatrix} \tag{4.2}$$

which represents Sun position in the Inertial reference frame centered at Earth-Moon barycenter, where $r_{\odot}$ is the Sun-Earth mean distance, $n_{\odot}$ is Sun mean angular velocity, t is time and ϵ is Earth orbit inclination around the Sun.

The resulting acceleration must also undergo a normalization procedure in order to be plugged in the equation of motion. The normalization has been performed

assuming constant characteristic quantities. Rigorously, this procedure should have been performed using θ-changing characteristic quantities, including time, but since accuracy on the disturbance is not the task of this work, computation has been simplified through this approximation. The normalization procedure is therefore performed as:

$$\hat{\vec{a}}_{SRP} = \vec{a}_{SRP} \frac{t^{*2}}{l^*} \tag{4.3}$$

where $\hat{\vec{a}}_{SRP}$ is the normalized acceleration due to Solar Radiation Pressure. It can be now plugged in the equation of motion, in order to have a more complete model of the orbital dynamic:

$$\begin{aligned}
\ddot{x} - 2\dot{y} &= \frac{1}{1 + e cos\theta}\left(\frac{\partial \Omega}{\partial x} + u_x + a_{SRP,x}\right) \\
\ddot{y} + 2\dot{x} &= \frac{1}{1 + e cos\theta}\left(\frac{\partial \Omega}{\partial y} + u_y + a_{SRP,y}\right) \\
\ddot{z} + z &= \frac{1}{1 + e cos\theta}\left(\frac{\partial \Omega}{\partial z} + u_z + a_{SRP,z}\right)
\end{aligned}$$

4.1.2 Errors

The possible injection errors that a spacecraft can incur into must be accounted for. This error has been modeled as a random, normally distributed component added to the initial condition, with zero mean and 100km standard deviation for position, 1m/s standard deviation for velocity. A control algorithm must be able to compensate for this error, but its main objective is the station keeping after the injection errors mitigation.

For this reason, when testing different control algorithms for many orbits, this error will not be introduced, since it may alter the results of the simulation. It will be validated afterwards, as a proof that the control algorithm can also be used to mitigate the injection error.

4.1.3 Performance Criteria

The following methodology is taken to evaluate the effectiveness of the controller. It was adopted by M. Zhu et al. [52] in his work on active disturbance rejection control. As suggested by him, the velocity increments ΔV (in unit of m/s/T), and the mean absolute value of the position errors are important parameters in determining the goodness of a control scheme.

The velocity increment can be computed as:

$$\Delta V = \frac{1}{T} \int_{t0}^{T} |u| dt \tag{4.4}$$

while the mean absolute position errors can be computed as:

$$e_i = |\Delta i|_{mean} \tag{4.5}$$

with $i = x, y, z$.

An other important parameters that can discriminate between different control algorithms is the time that can be dedicated to a scientific mission. As examples, Clementine NASA satellite required 1.5-2 hours of precise pointing during its mission phase of lunar imaging [10], while the Lumio spacecraft, a joint mission between ESA and Politecnico di Milano, currently under development, is expected to point at the far side of the Moon for up to half the Moon synodic period, $\approx$15 days [46]. The act and wait algorithm and the Schmitt trigger algorithm can be used to impose long periods of time where no control is achieved, thus allowing the spacecraft to point in the direction that the scientific mission requires. On the other hand, thanks to the conversion from continuous to impulsive control scheme, time between following maneuvers can be dedicated to the scientific mission, too. Careful must be paid in choosing the sampling frequency, since a smaller sample interval means a more frequent control action, which reduces idle time between following corrective maneuvers. For these reasons, two measures are selected as indices that represent the effectiveness of a control in delivering windows of free time: **longest window of no-control**, LW, and the **ratio between total no-control time over total simulated time**, R.

This particular choice has been made because the use of the longest window of no-control only would have made no use of the available time between impulsive maneuvers. It can add up to important values, in fact, depending on the particular discretization chosen, and therefore it would have not been able to provide the complete picture of a given control strategy. The same can be said for the ratio between total no-control time over total simulated time, because it can't provide a measure for the maximum and uninterrupted time available for a scientific mission.

It is therefore necessary to use both figures of merit.

4.1.4 Selected Thrusters

The two selected thrusters are here presented and discussed.

The chosen chemical thruster is the VACCO "ArgoMoon Propulsion System" [47], a hybrid propulsion unit composed by a main thruster of 100mN together with four smaller thrusters, 25mN each, for attitude maneuvering. The total unit mass, in a 1.3U format, is 2.065kg. The selected thrust level is 100mN, which corresponds to the main thruster only.

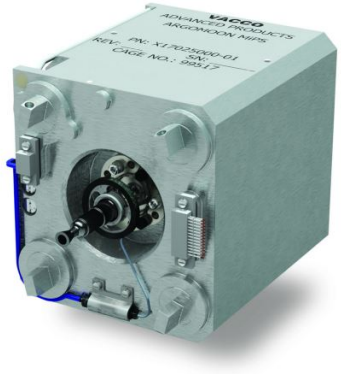

Figure 4.1: Vacco propulsion unit

The electric thruster selected is a 1U electric unit from Thrustme. the "NPT30-I2 smart propulsion with iodine propellant" [45] is a gridded ion thruster that used iodine as fuel. Its main advantage is its throttleable thrust, that can be exploited

to obtain a smoother control action. The chosen thrust level is therefore selected between 0.3mN and 1.1mN. The total wet mass is 1.2kg.

Figure 4.2: Thrustme propulsion unit

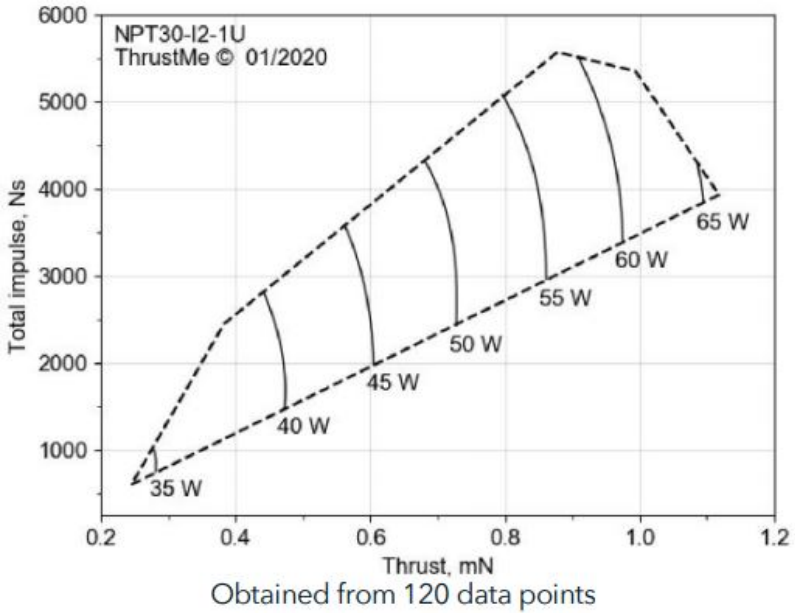

Figure 4.3: Thrustme propulsion unit thrust levels

Of course, since the simulation environment requires an acceleration, a mass hypothesis is required to convert thrust to acceleration. Since the propulsion systems together with the entire thesis work is tailored for cube-sat application, a generic mass of 24kg, suitable for a 16U cube-sat, is selected.

It is however necessary to convert the obtained acceleration in normalized units, in order to specify the maximum allowable acceleration coming from the thrusters. Moreover, due to the elliptical problem, the normalization process requires time-changing constants at each integration steps.

4.2 Results

4.2.1 Reference Trajectory Choice

The first important discriminant is the research of a suitable trajectory. As previously stated, two methodologies have been selected: one of them is based on the Fourier series approximation of a repeating orbit, while the other computes the orbit solving the ER3BP starting from an initial condition that produces a periodic orbit, which is then used as reference. It is expected that this last methodology produces a better result, because it eliminates the approximation that the Fourier series approach introduces. The Fourier series approximation does in fact impose the control to drive the spacecraft to a trajectory which is slightly different from the nominal one, which has instead been computed in order to minimize the control effort. Due to the instability of the L2 point, this new reference requires more station keeping cost.

It is also studied the difference in computing a reference trajectory in the CR3BP and in the ER3BP environment. Again, it is expected that the latter would produce a better result, because it uses a more realistic model.

For this simulation, a continuous control is chosen, without injection errors, in order to simulate a best-case scenario. The Fourier series parameters for the two orbits built in the CR3BP and ER3BP reference frames are listed in table 4.1, 4.2, 4.3 and 4.4.

coefficient	**X**	**Y**	**Z**
a_0	1.0856	1.9606e-18	7.3107e-02
a_1	4.2624e-02	5.7774e-07	1.2814e-01
a_2	1.8790e-06	-1.2764e-01	-7.6151e-07
a_3	-1.4276e-03	-1.6609e-07	-2.1764e-02
a_4	-1.2587e-07	1.8348e-02	2.5868e-07
a_5	-1.9045e-04	6.3373e-08	6.1803e-03
a_6	-2.5187e-08	-4.6670e-03	-1.1019e-07
a_7	2.3280e-04	-2.4843e-08	-2.2049e-03
a_8	4.1051e-08	1.3721e-03	5.2415e-08
b_1	-1.8185e-04	9.3143e-09	9.5998e-04
b_2	-4.0084e-08	-4.1156e-04	-2.8525e-08
b_3	1.2394e-04	-3.1097e-09	-4.6859e-04
b_4	3.2782e-08	1.1451e-04	1.6709e-08
b_5	-1.1559e-04	6.3271e-10	3.3080e-04
b_6	-3.5671e-08	-1.9969e-05	-1.3761e-08
b_7	9.6063e-05	2.6706e-10	-2.4243e-04
b_8	3.3879e-08	-7.3751e-06	1.1526e-08
ω	2.0000	2.0000	2.0000

Table 4.1: Fourier series coefficient for CR3BP orbital position

coefficient	**Vx**	**Vy**	**Vz**
a_0	-9.7467e-20	2.4532e-06	1.0296e-18
a_1	1.0391e-04	-2.5525e-01	-3.5992e-05
a_2	-8.5290e-02	-1.1732e-06	-2.5620e-01
a_3	-1.3768e-05	7.3380e-02	2.4488e-05
a_4	5.6500e-03	6.7452e-07	8.7157e-02
a_5	-3.9913e-06	-2.7975e-02	-1.5587e-05
a_6	1.0920e-03	-3.8573e-07	-3.6984e-02
a_7	9.0329e-06	1.0962e-02	9.8926e-06
a_8	-1.8535e-03	2.0152e-07	1.7604e-02
b_1	-1.0898e-05	-4.0895e-03	-6.7074e-06
b_2	1.7890e-03	-9.3979e-08	-9.5489e-03
b_3	1.0449e-05	1.3699e-03	4.6174e-06
b_4	-1.4294e-03	3.7777e-08	5.4780e-03
b_5	-1.2865e-05	-2.4770e-04	-4.3205e-06
b_6	1.5084e-03	-7.9692e-09	-4.3935e-03
b_7	1.4801e-05	-1.3714e-04	4.3121e-06
b_8	-1.5185e-03	-5.0426e-09	3.8368e-03
ω	2.0004	2.0000	2.0000

Table 4.2: Fourier series coefficient for CR3BP orbital velocity

coefficient	**X**	**Y**	**Z**
a_0	1.0929e+00	2.9540e-18	5.9463e-02
a_1	6.7818e-06	-6.6765e-18	3.4472e-02
a_2	4.0099e-18	-9.1346e-02	-3.3400e-18
a_3	5.8949e-02	-3.8082e-18	1.0407e-01
a_4	1.3501e-16	-1.1864e-01	-7.5943e-18
a_5	2.8574e-03	4.4279e-18	-3.5272e-02
a_6	8.5423e-18	2.8039e-02	-2.6342e-18
a_7	-7.2234e-03	5.2710e-18	-3.6207e-03
a_8	1.2783e-17	4.6542e-03	-1.6061e-18
b_1	1.7335e-03	2.0970e-18	9.7483e-03
b_2	1.5715e-17	-8.7948e-03	-1.9190e-19
b_3	1.5450e-03	-1.3129e-18	-3.7139e-03
b_4	-1.3299e-17	3.1380e-03	-3.7091e-19
b_5	-1.4116e-03	-8.9227e-19	-1.4630e-03
b_6	1.4663e-17	1.2962e-03	-2.6726e-18
b_7	2.2817e-04	3.1482e-18	2.0728e-03
b_8	-2.4955e-17	-1.9080e-03	3.2623e-18
ω	1.0282	1.0006	1.0016

Table 4.3: Fourier series coefficient for ER3BP orbital position

coefficient	**Vx**	**Vy**	**Vz**
a_0	-5.2321e-18	2.2938e-04	1.7683e-17
a_1	2.4329e-18	-9.0616e-02	-9.0374e-18
a_2	1.8949e-03	6.8991e-18	-3.5567e-02
a_3	-2.0134e-18	-2.3680e-01	6.0526e-18
a_4	-1.1984e-01	1.4559e-17	-2.0827e-01
a_5	5.5619e-18	8.3842e-02	7.6216e-18
a_6	-1.3516e-02	-5.2634e-18	1.0706e-01
a_7	-2.2767e-18	1.9838e-02	3.9545e-18
a_8	3.1175e-02	1.2247e-18	1.3126e-02
b_1	2.3896e-18	-4.3831e-02	-8.8753e-18
b_2	-7.2229e-03	-2.4067e-18	-4.9223e-02
b_3	-4.7805e-19	1.9246e-02	6.1421e-18
b_4	-1.0913e-02	2.9176e-18	2.2574e-02
b_5	4.5901e-19	9.8053e-03	1.9247e-18
b_6	9.5099e-03	-2.3743e-18	1.0082e-02
b_7	-5.4619e-18	-1.4947e-02	6.0600e-18
b_8	4.3381e-04	3.6147e-20	-1.7597e-02
ω	1.0158	9.9956e-01	1.0026

Table 4.4: Fourier series coefficient for ER3BP orbital velocity

The initial condition for the propagation of the reference orbit in case of reference trajectory through motion equation is instead the refined condition for the ER3BP orbit. This initial condition is also used as initial condition for spacecraft motion, while the initial conditions for the two Fourier-series approximated orbits are the corresponding approximation computed at $t = 0$. All the orbits are simulated for a time span equal to 8π, which corresponds to 4 orbits.

The diagram of position error and control actions reveal that the reference trajectory computed in this way allows a better error compensation (figure 4.4) and a reduced controlled effort (figure 4.6). Table 4.5 synthesizes the performance evaluation for the three orbits.

Orbit	**Velocity inc. [m/s/s]**	**Mean abs. err. [km]**
ER3BP ODE	5.185e-08	0.682
ER3BP Fourier	4.096e-04	4628.262
CR3BP Fourier	4.649e-04	5823.225

Table 4.5: Performance criteria with different reference trajectories

It is clear that a reference trajectory computed integrating the equation of motion provides a better reference for a spacecraft, due to the elimination of an approximation step. For the same reason, a reference computed including the effect of the eccentricity is better than a reference that doesn't consider it. It can be noted that only the trajectory computed through the integration of the equations of motion can provide an annual Delta-V below the requirement of 200m/s per year.

For this reason, the reference trajectory computed by integrating the equation of motion is selected as main reference.

Of particular interest is the entity of position and velocity error when using the reference defined as "main reference", which are bounded to a region of $\pm$1km and $\pm$5mm/s. These low values can be in fact misinterpreted for tracking errors, in a real scenario.

Lastly, for what concerns control effort, all the three methodologies allow the use of the chosen chemical thruster, since the maximum allowable acceleration coming

from this thruster amounts to 4.17x10^{-}3 m/s^2. On the other hand, the electric thruster can provide a maximum acceleration equal to 4.17x10^{-}5 m/s^2, which can only be achieved by the selected main trajectory.

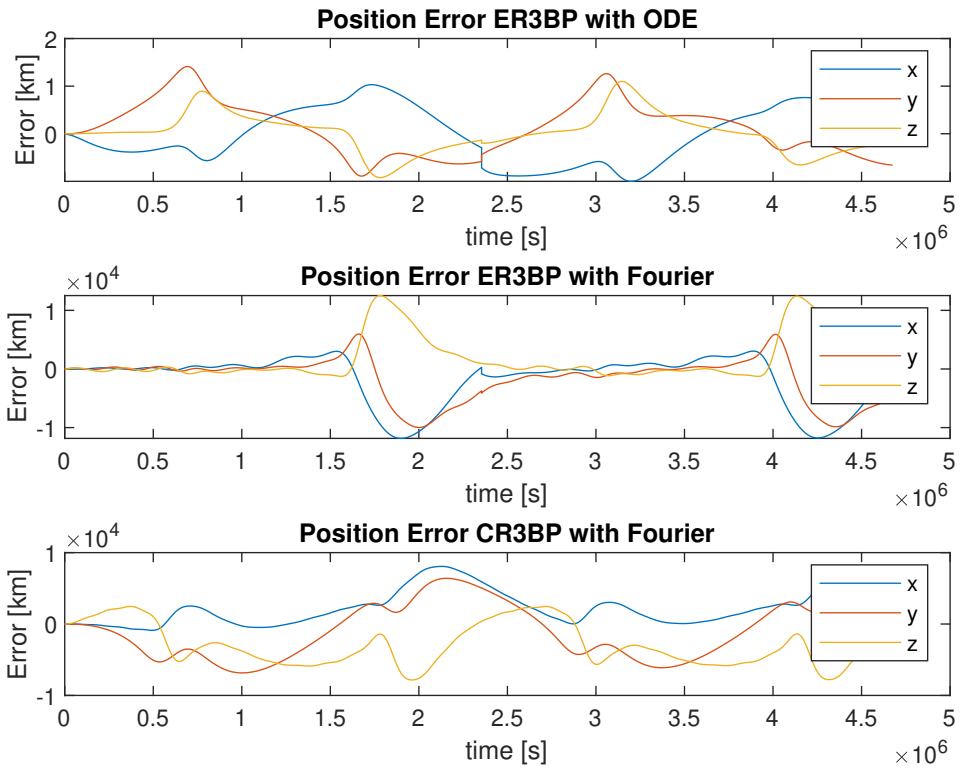

Figure 4.4: Position error with different reference trajectories

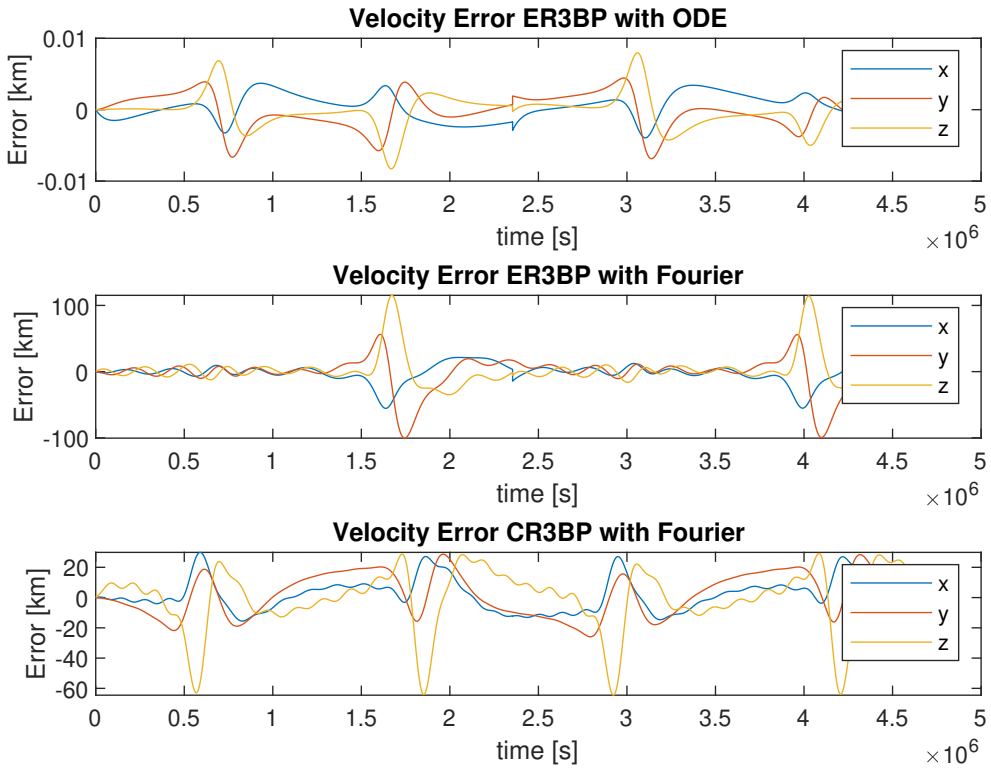

Figure 4.5: Velocity error with different reference trajectories

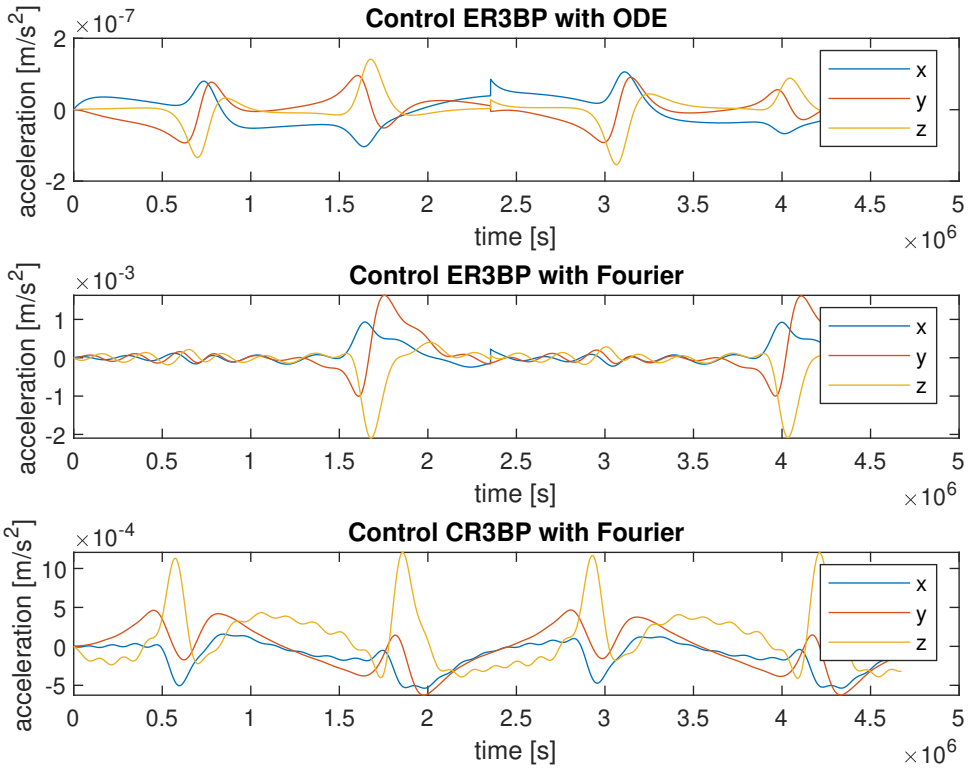

Figure 4.6: Control effort with different reference trajectories

4.2.2 Discrete Control

The next test involves the use of the discretized control, which can be helpful in the construction of an impulsive control. This control requires the tuning of the sample interval parameter T_s, which can affect the performance of the station-keeping, and must be compared with a classical continuous LQR. The simulation has been performed along a time span of normalized time equal to 2π, without considering injection errors. The three choices for T_s have been selected as $\pi/200$, $\pi/100$ and $\pi/50$, which correspond to an updating interval of ≈1.5h, ≈3h and ≈6h, respectively.

As it can be noted by table 4.6, the mean absolute error is very similar between all the four cases, while the velocity increment, which is linked to ΔV usage, increase by 0.28% when moving from a continuous control to a discretized control with $T_s = \pi/200$ and by 0.23% when moving from $T_s = \pi/200$ to $T_s = \pi/100$. The same increment reaches 0.92% when introducing $T_s = \pi/50$. In any case, the behaviour of both the position and the velocity error is similar, with all the three discretized control cases achieving stable station-keeping.

Control	**Velocity inc. [m/s/s]**	**Mean abs. err. [km]**
Continuous	3.884e-8	0.111
Discrete ($T_s = \pi/200$)	3.895e-8	0.100
Discrete ($T_s = \pi/100$)	3.904e-8	0.100
Discrete ($T_s = \pi/50$)	3.940e-8	0.101

Table 4.6: Performance criteria with different control types

Due to the different sample time, the shape of the control action is different, and this can be noted in figure 4.11, where a smaller sample time interval makes the control action behave more like a control action from a continuous control. The same choice affects the computational time, where a greater sample time makes the simulation faster, due to the lower control frequency.

The achieved acceleration, for all the considered cases, is compatible with the chosen thrusters.

Given these considerations, the value of $T_s = \pi/100$ has been chosen as a good compromise between computational accuracy and effort for a discretized control.

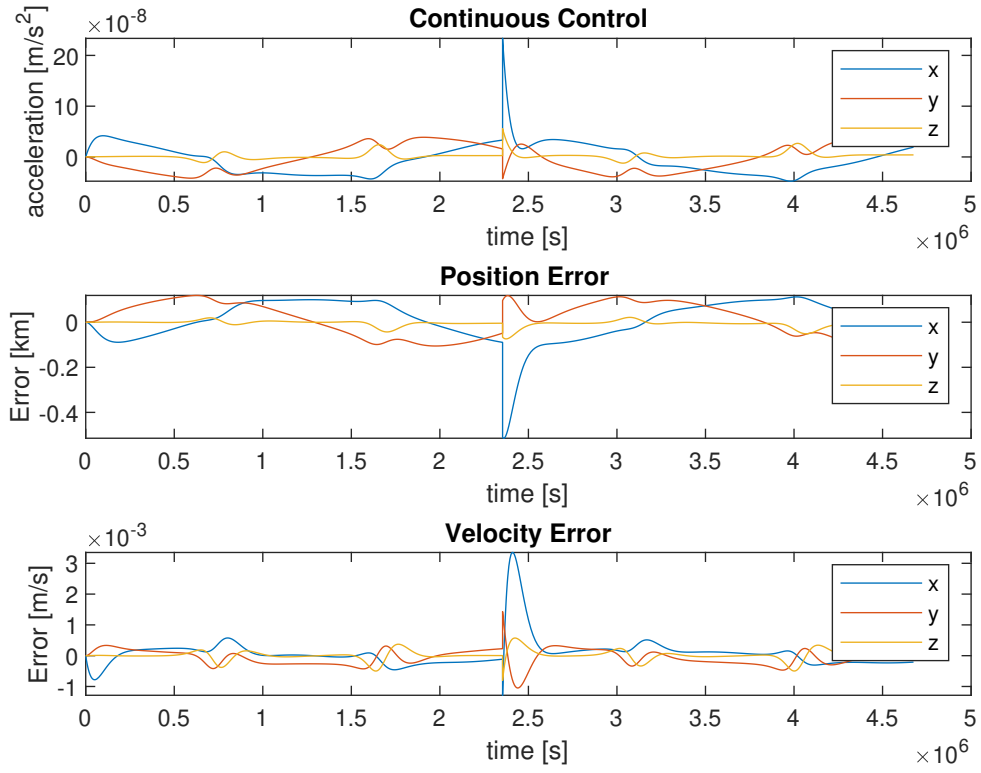

Figure 4.7: Results from continuous control

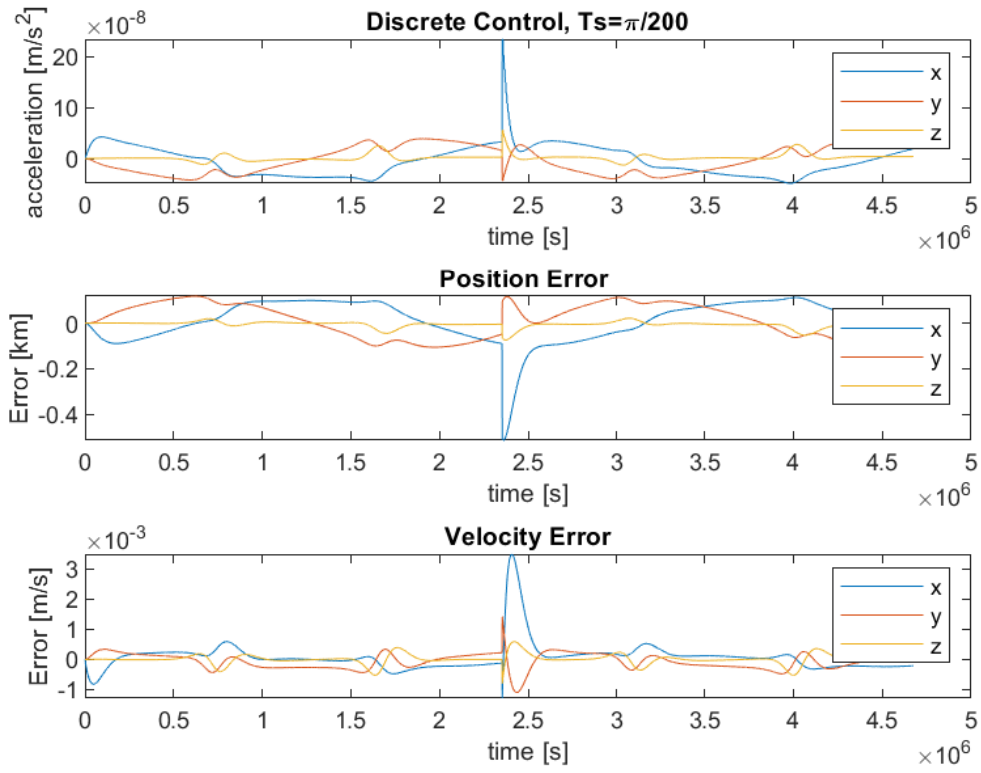

Figure 4.8: Results from discrete control with $T_s = \pi/200$

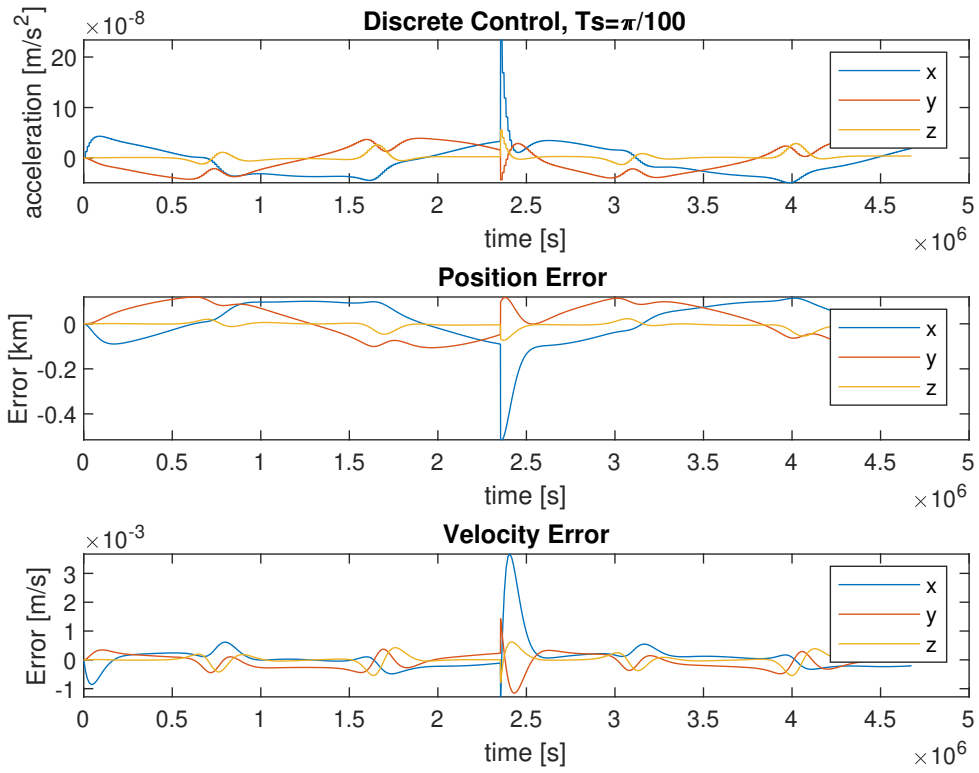

Figure 4.9: Results from discrete control with $T_s = \pi/100$

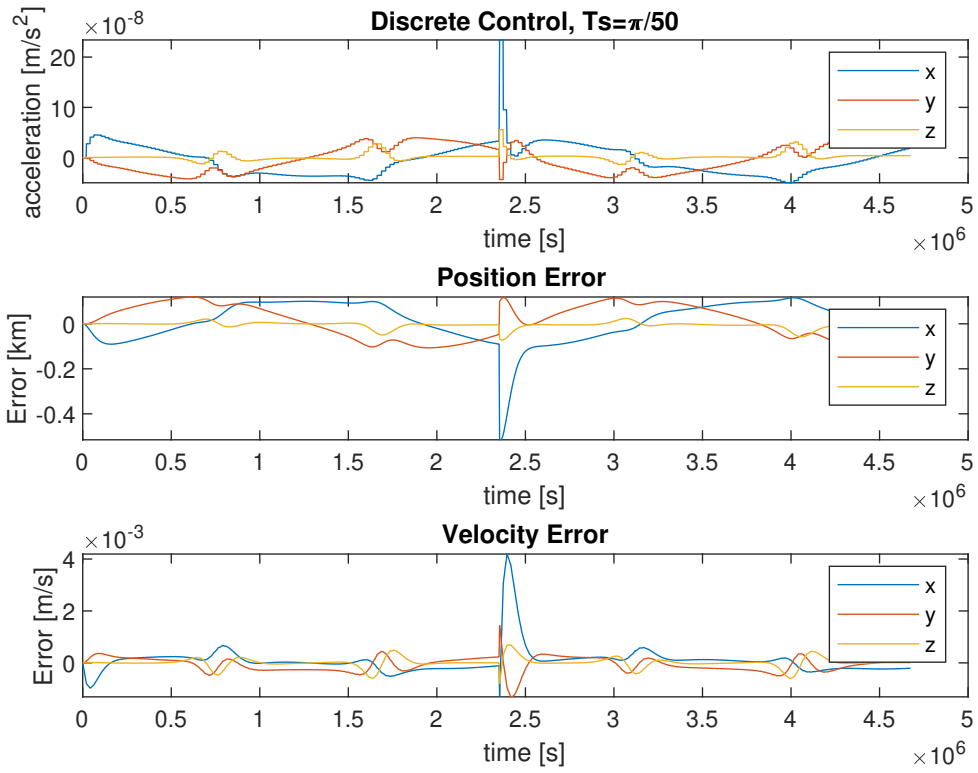

Figure 4.10: Results from discrete control with $T_s = \pi/50$

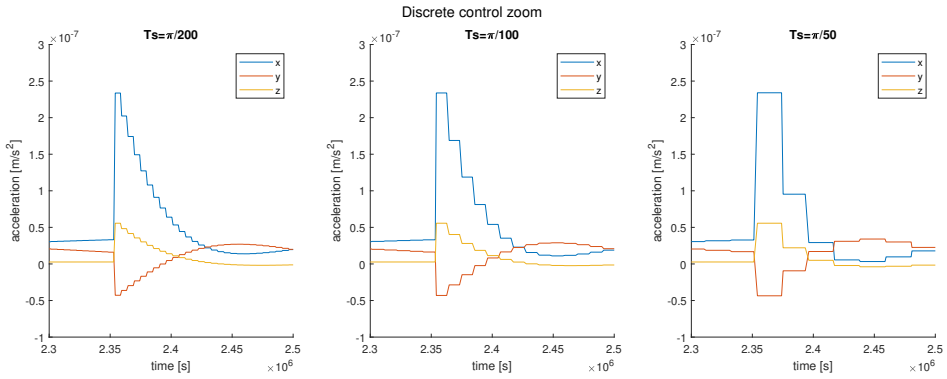

Figure 4.11: Detail on a same spot with different T_s

4.2.3 Proportional Derivative Control

This test evaluates the use of a proportional derivative control for orbit maintenance. No injection error is yet introduced and the simulation is tested over a period of two orbits with a discretized control (T_s=$\pi/100$). This section is also used to find a suitable value for the derivative gain k_p.

The result are summarized in table 4.7. It can be noted that the mean absolute error is similar between the different cases, while the Delta-V requirement is actually improving as the proportional gain k_d is increasing, following a rule of decreasing increments.

Control	**Velocity inc. [m/s/s]**	**Mean abs. err. [km]**
$k_d = 0$	3.904e-8	0.100
$k_d = 0.1$	3.863e-8	0.101
$k_d = 0.2$	3.839e-8	0.101
$k_d = 0.3$	3.820e-8	0.101
$k_d = 0.4$	3.807e-8	0.100

Table 4.7: Performance criteria with different derivative gains

The practical benefit of a proportional discrete control is shown in figure 4.12 and 4.13, where two simulations are run with an injection error. It can be noted that

the use of a simple LQR produces a control that oscillates when large corrections are required. This behaviour is solved with the introduction of a derivative component.

It can be concluded that the introduction of a derivative component in the control is useful in improving the control behaviour and thus the Delta-V requirement. It is however not possible to select an optimal value for the derivative gain, since the simulation is lacking important strategies such as impulsive control or the Schmitt trigger, which can alter the control behaviour and make it more discontinuous. Moreover, the simulation is still lacking in realism, since no constrain on the acceleration or on the error is introduced.

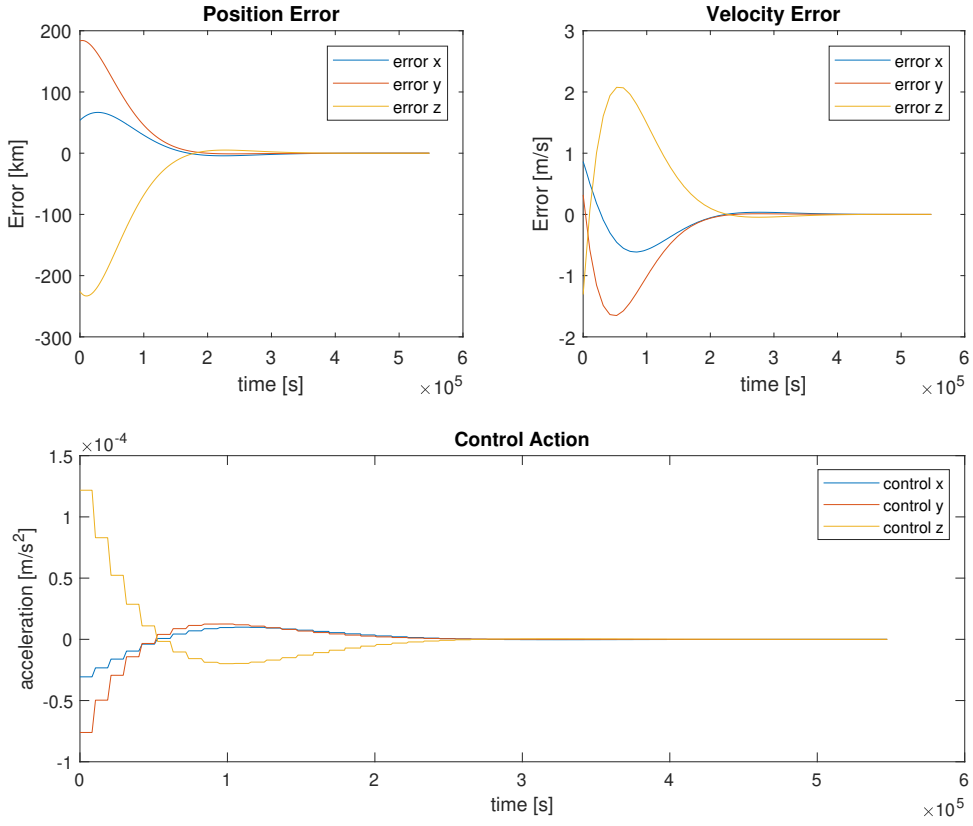

Figure 4.12: Results from discrete control with $k_d = 0$

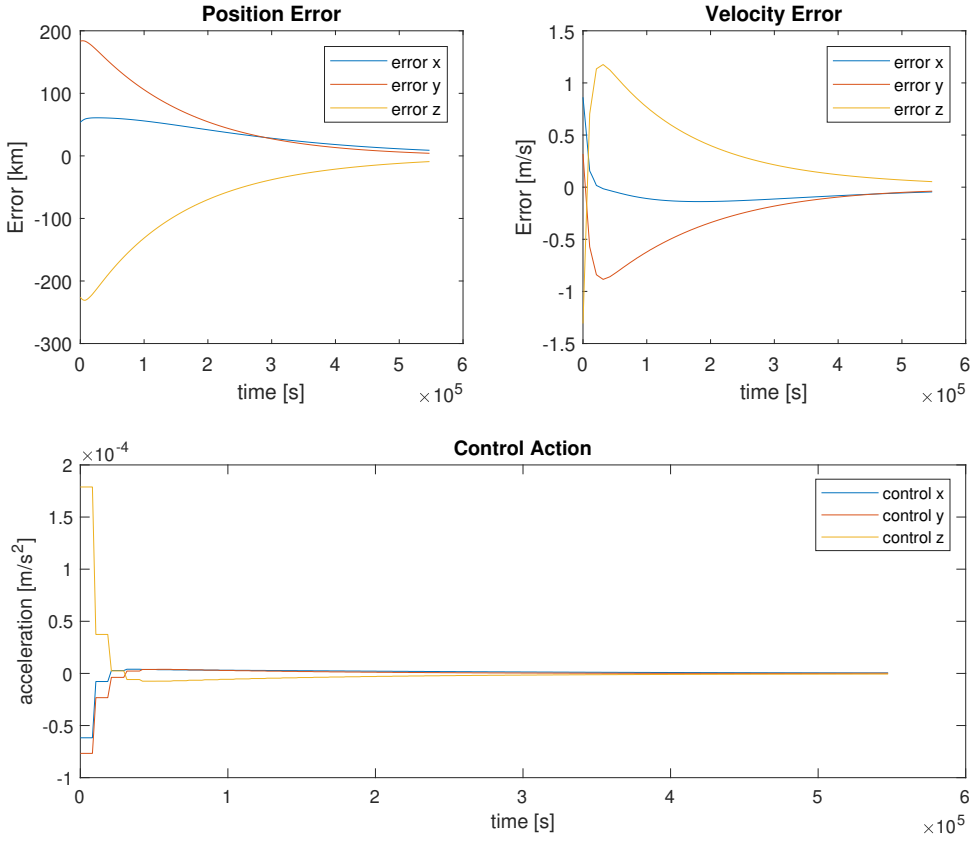

Figure 4.13: Results from discrete control with $k_d = 0.3$

4.2.4 Act-and-Wait Control

This section applies the Act-and-wait strategy to the control, together with the impulsive discrete transformation of the nominal control. Here, the real values of the available accelerations are for the first time introduced, and a more realistic scenario is therefore simulated. In order to consider the real performance this control technique has on the station keeping, which is analyzed over a time span of two orbits, the injection error is introduced, which acts as an error that have increased after a previous waiting phase. An analysis on the weight of the derivative gain k_d is performed, for both thrusters. Moreover, since the Schmitt trigger has a lower bound on the error state under which the control deactivates, a similar lower bound is here introduced: if the position error is below 5km and the velocity error is below 0.1m/s, no control is performed. Lastly, a waiting time t_w of 2 minutes is introduced, which is a reasonable value for an attitude maneuver.

The first batch of results adopts the chemical thruster. Two cycles t_c of π and 2π are developed, which correspond to two control phases along one orbit and only one control phase per orbit, respectively. The act time t_a, after many iterations, has been found to be equal to at least $\pi/3$ for the first case and $2/3\pi$ for the second, otherwise the control would diverge. Since the developed model is limited for what concerns perturbances and disturbances, an augmented act time t_a equal to $\pi/2$ and π has been chosen, in order to allow for some robustness in case of a more realistic scenario.

The results are listed in table 4.8, where also the performance criteria about longest window of no-control and the ratio between total no-control time over total simulated time. The abbreviations V inc. and m.ab.E stand for velocity increment and mean absolute error. As a first regard, it can be appreciated how the chemical thruster requires less than 1% of the total mission time to provide a stable station keeping, independently on the choice of the parameters.

n	t_c	k_d	**V inc. [m/s/s]**	**m.ab.E [km]**	**LW [days]**	**R [%]**
1	π	0	$7.952\text{x}10^{-6}$	120	7.6	99.81
2	π	0.1	$5.093\text{x}10^{-6}$	108	10.8	99.88
3	π	0.2	$3.866\text{x}10^{-6}$	84	8.2	99.91
4	π	0.3	$3.576\text{x}10^{-6}$	68	9.5	99.92
5	π	0.4	$5.283\text{x}10^{-6}$	40	9.8	99.87
6	2π	0	$1.234\text{x}10^{-5}$	359	11.0	99.71
7	2π	0.1	$2.164\text{x}10^{-5}$	781	16.7	99.48
8	2π	0.2	$1.255\text{x}10^{-5}$	659	16.1	99.70
9	2π	0.3	$1.182\text{x}10^{-5}$	529	16.4	99.72
10	2π	0.4	$2.458\text{x}10^{-6}$	103	16.4	99.94
11	2π	0.5	$8.432\text{x}10^{-6}$	336	16.7	99.80

Table 4.8: Act-and-wait control with different settings, chemical thruster

It can be noted that, for the π-cycle, an increase in derivative gain brings benefits in terms of fuel requirement, mean absolute error and ratio R, up to a certain value, where performances start to decrease. In this case, the longest window of no control is found for a value of k_d equal to 0.1, which allows up to 10.8 days without acting on the station keeping, while the best ratio between total no-control time over total simulated time is found for a value of k_d equal to 0.3, which also corresponds to the case with the least velocity increment. For this case, total Delta-V requirement over one year would amount to 113 m/s.

For the cases with t_c equal to 2π the increase of cycle duration has a great effect on the mean absolute error, due to the fact that the position error is allowed to increase for a greater amount of time. It can be noted that there is an initial worsening of the performance as the derivative gain increases, a part for the longest window of no control which is actually improved, up to a certain value of k_d, where instead a local minima for fuel requirement, mean absolute error and ratio R is found. The longest window of no control is instead slightly smaller than the maximum, and it's equal to 16.4 days. For this case, namely k_d=0.4, annual Delta-V budget amounts to 78 m/s.

It can be noted how this case offer the best fuel requirement and the best scientific performances, even better than the shorter π-cycle, which should, in theory, allow a more frequent control and thus a smaller error increase, with consequently less Delta-V. It has been found that a numerical bug causes this issue.

This bug is a combined effect of the short pulse duration of the chemical rocket engine, due to its high thrust, and the length of the waiting time t_w. For some cases, particularly at the end of the control window, where the error is small, it is possible that the pulse duration for a discretized interval is much smaller that the waiting time. The simulation is able to compute the duration of the pulse d, which can reach values below one second, but it's not able to dynamically adjust its resolution, which is instead automatically calibrated for 2 minutes. Therefore, the control skips the control interval. Reducing the discretization level, in an attempt to obtain a less frequent control action and thus an increased error, doesn't solve the problem, and it is actually partially mitigated by an increase in cycle time. This is why the best case for the chemical thruster is found for the 2π-cycle, where the error is allowed to increase to a much higher entity.

Figure 4.14 shows important plots for case 10), the one with the best overall performance, with a detail on the control norm, where the impulsive behaviour can be appreciated. As an example, the control has computed that the first control pulse at the beginning of the second control phase would require 870s of continuous thrust, while the last control impulse would require only 38s. It can also be noted how the control achieves an acceleration equal to the one imposed by the particular thruster, namely a=0.0417 m/s^2.

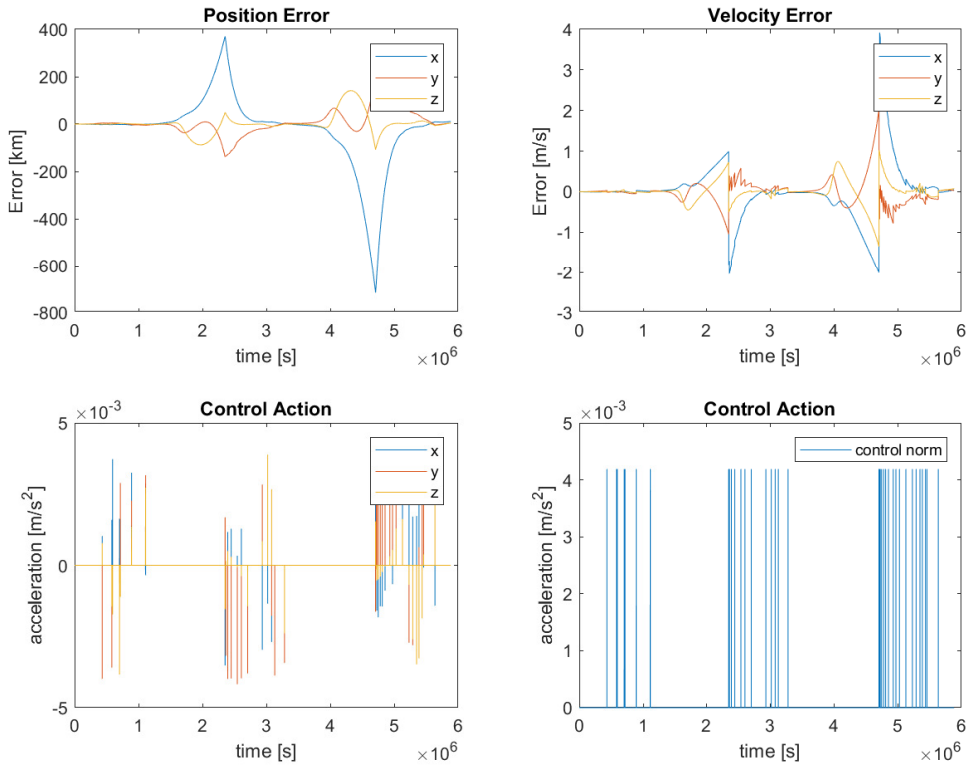

Figure 4.14: Chemical thruster with $t_c = 2\pi$ and $k_d = 0.4$

The result coming from the electric thruster are listed in table 4.9. The same values of the previous one are adopted, for what concerns cycle duration and waiting time. It can be noted how, case by case, the fuel requirement is smaller for the electric thruster than the chemical one, thanks to its smaller thrust level which achieves a smoother control action.

Similarly to what happened for the chemical thruster for the π-cycle, an increase of the derivative gain provides a general increment in station keeping performance. Only the longest window of no control appears to behave in an opposite manner, with a reduction of its size as k_d increases. In this case, a trade-off is necessary to select the best case, depending on the mission constrains, as some cases allows better station keeping cost at the expense of the size of the no control window.

n	t_c	k_d	**V inc. [m/s/s]**	**m.ab.E [km]**	**LW [days]**	**R [%]**
12	π	0	$3.793\text{x}10^{-6}$	49	9.8	78.87
13	π	0.1	$2.826\text{x}10^{-6}$	51	9.4	84.26
14	π	0.2	$2.242\text{x}10^{-6}$	46	8.0	87.52
15	π	0.3	$1.727\text{x}10^{-6}$	46	7.9	90.38
16	π	0.4	$2.479\text{x}10^{-6}$	57	9.0	86.20
17	2π	0	$2.157\text{x}10^{-6}$	39	13.9	87.99
18	2π	0.1	$3.177\text{x}10^{-6}$	95	15.3	82.30
19	2π	0.2	$1.251\text{x}10^{-6}$	54	17.4	93.03
20	2π	0.3	$1.360\text{x}10^{-6}$	56	16.6	92.43

Table 4.9: Act-and-wait control with different settings, electric thruster

For the 2π-case, the results are similar to the π-cycle. Fuel requirement, mean absolute error and ratio R are similar, while there is a great improvement over the window of no control. For this reason, there is no doubt that a control cycle of period 2π provides a better control architecture. It can also be noted that a clear, better derivative gain is detectable, namely k_d=0.2, which allows the best annual Delta-V budget, 40m/s, the best window of no control, 17.4 days, and the best ratio of total no-control time over total simulated time.

The resulting graph of this case are listed in figure 4.15 . It can be noted how the control requires longer control pulses, as big as the entire discretized interval, minus the waiting time, which has an effect over the ratio R. These control pulses appear as if the control was continuous, but a detailed zoom over the second control phase, however, shows how the control is actually impulsive (figure 4.16). It can also be noted how the control norm is bounded between the maximum acceleration, $4.17\text{x}10^{-5}$ m/s^2, and the minimum one, $1.39\text{x}10^{-5}$ m/s^2. Lastly, at the beginning of the second control phase, the first required impulse is 8100s long, while the last control impulse is 191s long.

As final notes, the electric thruster, due to its lower thrust level, requires longer control pulses, which, depending on the free parameters, require up to 22% of the

total simulated time. On the other hand, the fact that the control pulses are much longer makes the simulation safe from the numerical bug that afflicted the chemical thrust. This consideration, together with the smoother control behaviour, can explain the reduced fuel requirement for the electric thruster.

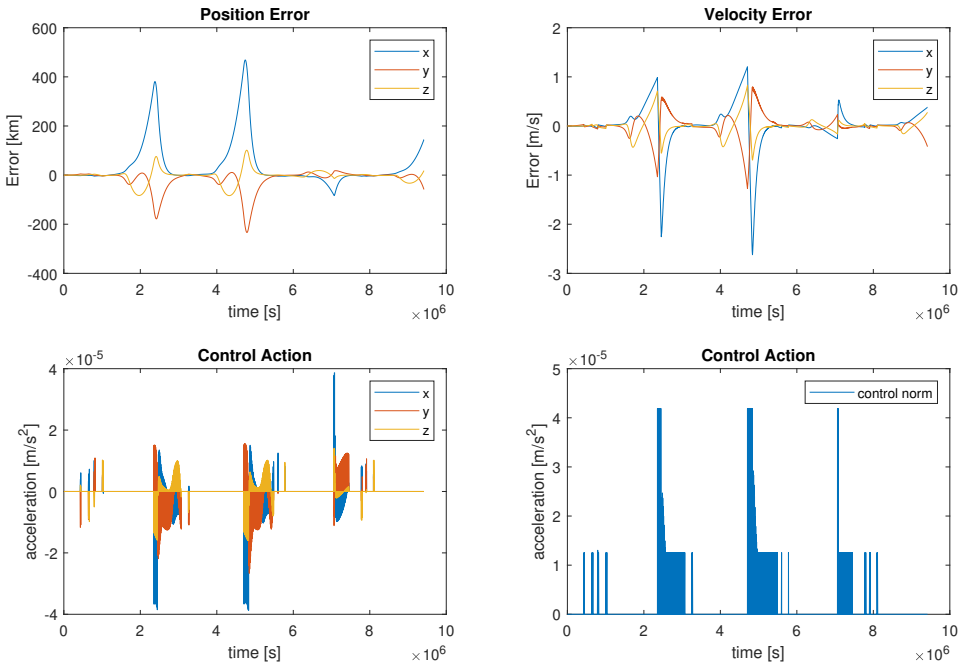

Figure 4.15: Electric thruster with $t_c = 2\pi$ and $k_d = 0.2$

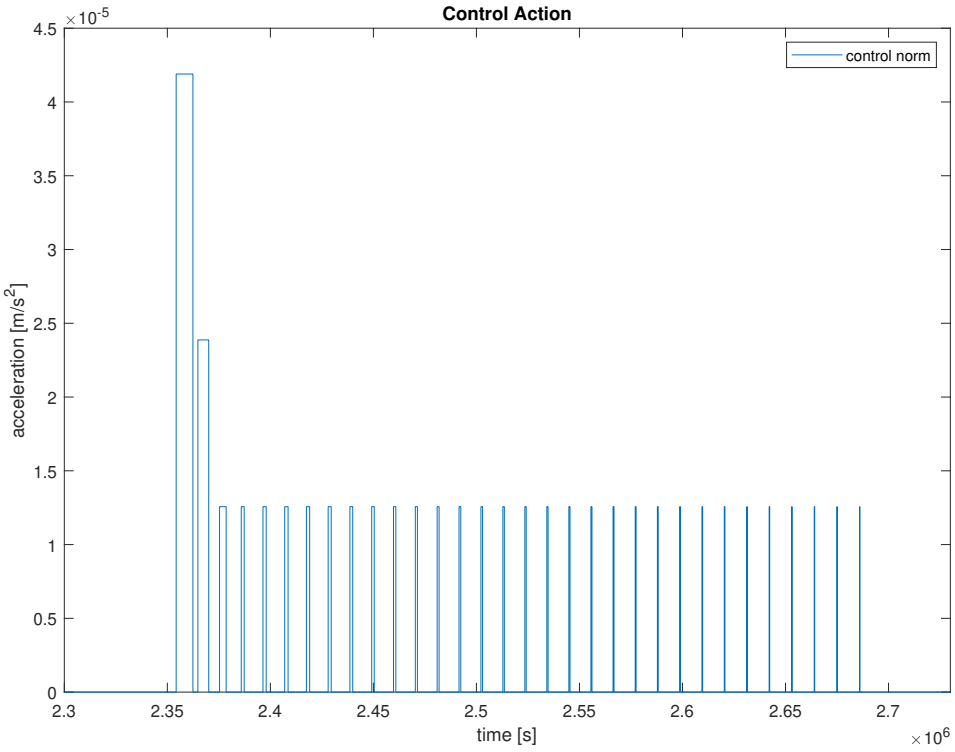

Figure 4.16: Detail over the second control phase

4.2.5 Schmitt trigger

As previously stated, a different way to activate and deactivate the control can be based on the error state, rather than on time, thanks to the Schmitt trigger. The definition of the boundaries, however, requires the tuning of the weight k, and the identification of suitable upper and lower boundaries. The weight has been chosen in such a way that, in normalized terms, a position error of 100km would have the same importance as 2m/s of velocity error, namely k=0.13. Then, the upper boundary have been chosen in such a way that a certain position error alone or a velocity error alone would activate the control, for example 100km and 0m/s or 0km and 2m/s of

error which, in normalized values, corresponds to 2.6x10^{-4}. The lower boundary has been instead selected in such a way that the position and velocity error must not surpass a combined error, in normalized values, of 2.6x10^{-5}, which corresponds to 5km and 0.1m/s of error, combined.

The value of the normalized boundaries should vary in time, due to the elliptical problem, but a constant value is preferred to make the computation of spacecraft motion easier.

Different upper boundaries are therefore tested for both thrusters. The value of the derivative gain is not however tested, and the appropriate value has been chosen as the best case that each thruster achieved in the act-and-wait algorithm. The simulation is two orbits long and the injection error is again introduced to simulate the end of a previous waiting phase.

The results are listed in table 4.10 for the chemical thruster and in table 4.11 for the electric thruster. The abbreviation "ub" stands for "upper bound" and represents the equal amount of position or velocity error that activates the control.

It can be noted that for both thrusters, an increase in upper bound level decreases the station keeping performance, requiring more Delta-V budget due to the progressive increase of the error state. For the chemical thruster, however, this behaviour has little effect on the ratio R, while it actually allows a bigger window of no control as the upper bound increases. Case 23) allows up to 12 days of no control, at the expense of fuel requirement, 193 m/s of annual Delta-v budget, which is however within the margin of 200m/s per year. The diagrams of this case are represented in figure 4.17 and it can be seen how there are more windows of no control, albeit smaller than the maximum, with respect to the act and wait control which only had one, bigger window. This configuration possesses therefore exploitation that can be used. On the other hand, a more frequent control with a lower upper threshold like case 21) is able to save more than half fuel requirement, at the expense of half of the maximum window of no control, which is suitable for a longer mission duration. The final choice between the two must therefore undergo a selection based also on the mission scientific requirements.

n	ub [km - m/s]	V inc. [m/s/s]	m.ab.E [km]	LW [days]	R [%]
21	50 - 1	$2.646\text{x}10^{-6}$	37	6.3	99.94
22	100 - 2	$4.989\text{x}10^{-6}$	64	7.6	99.88
23	200 - 4	$6.122\text{x}10^{-6}$	99	12.0	99.88
24	300 - 6	$1.202\text{x}10^{-5}$	170	5.7	99.71

Table 4.10: Schmitt trigger with different settings, chemical thruster

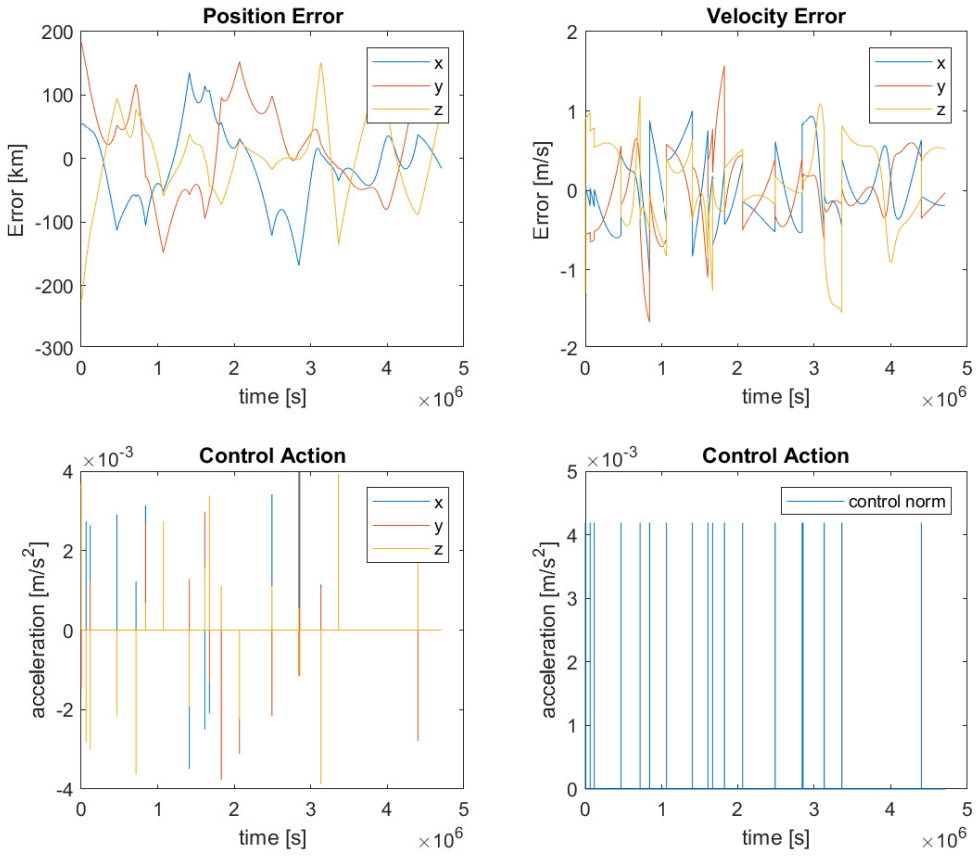

Figure 4.17: Schmitt trigger control with case 23) of chemical thruster

The electric thruster is penalized by this kind of control, due to its low thrust level which requires much more time than the chemical thruster in order to maintain the Halo orbit. It can be indeed noted that the best performance is achieved when the upper bound is set to a low value. Paradoxically, due to the lower required control effort offered by this solution, the electric thruster requires less time to correct the error, thus allowing a greater window of no control. Also the ratio of total no-control time over total simulated time is the best for this case. The diagrams of this case are represented in figure 4.18. It can be noted that, a part for the first control phase where the engine is working to resolve the injection error, the electric thruster action is more impulsive and less frequent in time, with respect to the act and wait control which instead was more frequent in the control phase. Similarly to the chemical thruster, there are frequent windows where the engine is not operative that can be exploited, if the scientific mission allows their use.

n	**ub [km - m/s]**	**V inc. [m/s/s]**	**m.ab.E [km]**	**LW [days]**	**R [%]**
25	50 - 1	$2.785\text{x}10^{-6}$	58	6.0	84.49
26	100 - 2	$5.136\text{x}10^{-6}$	82	4.9	71.40
27	200 - 4	$9.595\text{x}10^{-6}$	138	4.0	45.56

Table 4.11: Schmitt trigger with different settings, electric thruster

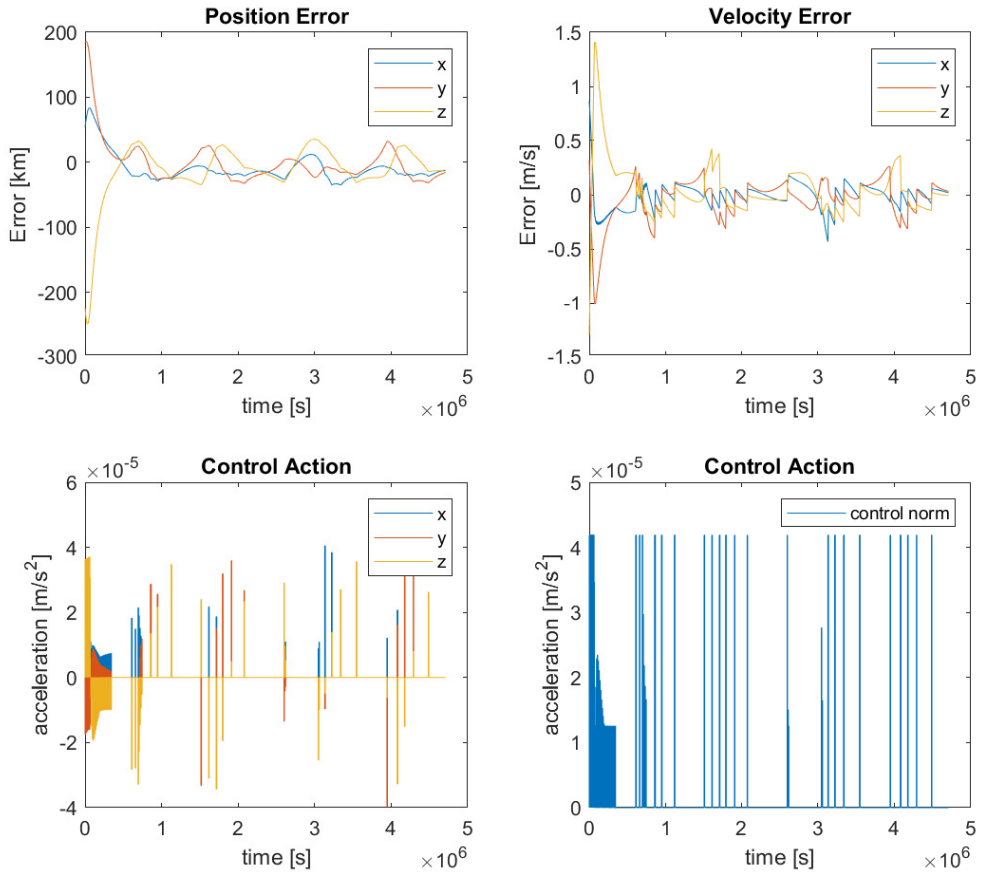

Figure 4.18: Schmitt trigger control with case 25) of electric thruster

The Schmitt trigger logic can also be applied separately on the three main axis in such a away that when an axis doesn't need to be controlled all the thrust can be dedicated to the remaining two. This implementation can help the electric rocket engine, due to its lower thrust.

The results from this kind of different implementation for the chemical thruster are listed in table 4.12 . It can be noted that there is an overall decrease in the performance, with respect to the Schmitt trigger based on the overall error, when implementing this kind of control. Case 29) and 30) are in fact above the limit of 200m/s of annual Delta-V budget, therefore only case 28) is suitable for a real mission. It has however almost double fuel consumption and a lower longest window of no control with respect to a simpler Schmitt trigger.

n	**ub [km - m/s]**	**V inc. [m/s/s]**	**m.ab.E [km]**	**LW [days]**	**R [%]**
28	50 - 1	$4.201\text{x}10^{-6}$	44	5.7	99.80
29	100 - 2	$6.400\text{x}10^{-6}$	71	5.8	99.85
30	200 - 4	$8.770\text{x}10^{-6}$	119	9.8	99.79

Table 4.12: Schmitt trigger with different settings, separately applied on the three axis, chemical thruster

As an example, selecting case 30), which has the same upper bound as previously done, it can be noted how the control is more frequent, thus reducing the possibility of achieving long periods of time without control (figure 4.19)

The situation is instead different selecting the electric thruster, as it can be noted in table 4.13. The best overall result is given by case 31), since case 32) is close to the annual maximum Delta-V budget and case 33) surpasses it. The possibility of dedicating the lower thrust to a reduced number of axis allows this particular engine to perform its correcting maneuver in less time than with a Schmitt trigger based on the overall error state. This situation has a beneficial effect on the maximum window of no control, since it's now comparable to the one obtained with the chemical thruster. The downside in this different control logic is given by the fact that more control impulses are required, thus increasing the overall fuel requirement. The

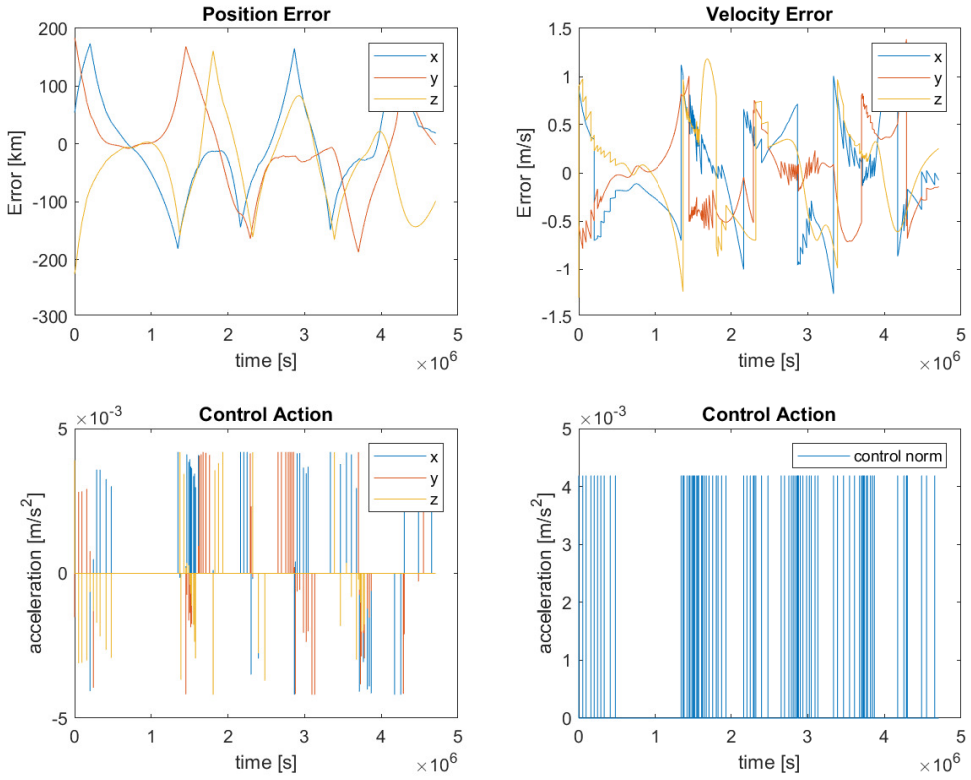

Figure 4.19: Separate Schmitt trigger control with case 3) of chemical thruster

Schmitt trigger separately applied over the three axis has sensibly improved the scientific criteria with respect to a simpler Schmitt trigger control, at the expense of an increase 13% in station-keeping cost. The results of case 31) are shown in figure 4.20.

n	ub [km - m/s]	V inc. [m/s/s]	m.ab.E [km]	LW [days]	R [%]
31	50 - 1	$3.152\text{x}10^{-6}$	46	8.0	96.02
32	100 - 2	$5.790\text{x}10^{-6}$	67	9.1	93.07
33	200 - 4	$9.786\text{x}10^{-6}$	103	8.5	87.12

Table 4.13: Schmitt trigger with different settings, separately applied on the three axis, electric thruster

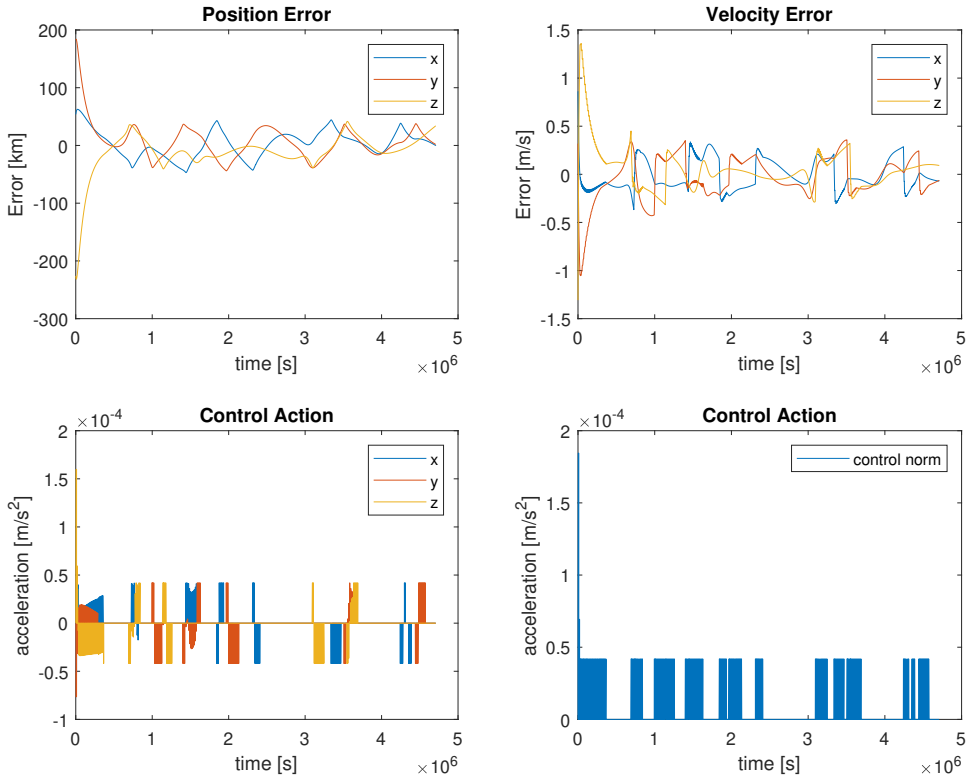

Figure 4.20: Separate Schmitt trigger control with case 1) of electric thruster

Chapter 5

Conclusion

The developed thesis has demonstrated that it is possible to obtain a control that allows windows of free time where no control is active, while, at the same time, achieving a stable station-keeping in the unstable motion around L2 Lagrangian point. The results are also compatible with the Cubesat standard, since they have been obtained using commercially available Cubesat engine data.

Table 5.1 provides a quick summary of the most performing results. The abbreviations Aaw, St, sSt stand for act-and-wait, Schmitt trigger and separate Schmitt trigger. It is also chosen to show the total annual Delta-V requirement instead of the velocity increment, as it is a more immediate information. The parameter ub stands for "upper bound" and in the table it is written the corresponding position error and velocity error that alone cause the Schmitt trigger to activate. The distinction between different thruster is given by the letter: C for chemical thruster and E for electric thruster.

Judging by the results alone, it may appear that a control based on time is more efficient than a control based on error, under every aspect of a space mission, from fuel requirement to time available for the scientific mission. It must be however remembered that the intrinsic drawback of the act-and-wait control is the proper selection of the active time t_a, which affects the convergence of the station keeping. The Schmitt trigger is exempted by this drawback, due to its error-based mechanism,

Case	Thruster	Control type	Parameter	k_d	Delta-V annual [m/s]	m.ab.E [km]	LW [days]	R [%]
4	C	AaW	$t_c = \pi$	0.3	113	68	9.5	99.92
10	C	AaW	$t_c = 2\pi$	0.4	78	103	16.4	99.94
21	C	St	ub = [50km, 1m/s]	0.4	83	37	6.3	99.94
23	C	St	ub = [200km, 4m/s]	0.4	193	99	12	99.88
28	C	sSt	ub = [50km, 1m/s]	0.4	133	44	5.7	99.80
15	E	AaW	$t_c = \pi$	0.3	55	46	7.9	90.38
19	E	AaW	$t_c = 2\pi$	0.2	40	54	17.4	93.03
25	E	St	ub = [50km, 1m/s]	0.2	88	58	6.0	84.49
31	E	sSt	ub = [50km, 1m/s]	0.2	99	46	8.0	96.02

Table 5.1: Best performing simulations

which is actually better suited for the unstable mission to the L2 point of the Earth-Moon system. An other important factor for this control is the robustness, its ability to react in case of unforeseen disturbances and modelization errors, which is not embedded in the act-and-wait control logic. The Schmitt trigger, however, doesn't allow a precise schedule of mission time, due to the unpredictability of possible disturbances and the instability of the Halo orbit, which is instead guaranteed by the act-and-wait control logic. Therefore, careful consideration must be paid in the choice of the control algorithm. The main driver for this choice is represented by the scientific requirements, which can provide information about mission timing and planning.

The act-and-wait algorithm is also best suited for a case where a longer period

of time is dedicated to the waiting phase, since both thrusters are able to obtain the best overall performance in correspondence of the 2π-cycle, with only one control phase per orbit.

The Schmitt trigger logic is instead best suited for a chemical thruster when it considers the overall position and velocity error, due to the fact that this thruster is able to provide a higher acceleration than the electric thruster. On the other hand, this particular engine is best suited for a Schmitt trigger which acts separately on the three axis, thanks to its thrust partitioning peculiarity, which mitigates the intrinsic low acceleration provided by the electric thruster.

It is however clear that the implementation of a proportional-derivative control allows the construction of a more efficient control that mitigates the oscillating behaviour typical of a simple proportional control. Without this contribution, the task of achieving long periods of time with no control action would have been severely hampered.

The introduction of a transformation that modify the control from continuous to impulsive has also made possible the exploitation of free time between different maneuvers. At the same time, it has allowed the construction of a more realistic scenario, with thrust levels coming from real rocket engines data sheets and the possibility to account for attitude maneuvers. The discretization of the control as a first, important step has been fundamental in achieving this transformation, which can also be expanded and further analyzed in future works.

From a thruster point of view, the results state that a chemical thruster is more suitable for correcting large errors, thanks to the increased provided acceleration, while an electric thruster, with its more modest thrust, is able to achieve a smoother control, with benefits on the maintenance of the orbit in terms of Delta-V budget. The choice of the two thrusters must also take into account the difference in the overall system. A chemical rocket engine does in fact require more fuel than an electric one, due to the lower specific impulse, which instead requires larger solar arrays due to the higher power requirement. Both cases must therefore undergo a crucial analysis, due to the involved mass behind the two thrusters that can affect the overall space system mass and design.

From the work done, it has been noted how the study of motion around Lagrangian points requires the use of the most realistic simulation, avoiding, if possible, too many approximation. This has clear remarks when evaluating a suitable reference trajectory, where the use of the elliptical restricted 3-body problem and the avoidance of the Fourier series provided a better trajectory in terms of station keeping cost and effort.

Future work can implement different orbits, which may behave in different manners than the one developed and studied. A complete mission analysis, with Earth-Moon transfer orbit and end of life disposal of the space system could also be a possible improvement. A coupled attitude-orbital dynamic could also improve the accuracy of the model, particularly for what concerns the choice of the waiting time before a control pulse. The main difficulty in this process is given by the different time scale at which these two dynamics work, since, in normalized units, the orbital dynamic is 375,704 times faster than the attitude dynamic. An other improvement can be made by introducing more perturbations, like the J2 effect of the moon or the influence of other, influential bodies in the solar systems, such as the Sun. Moreover, a procedure of optimization can be performed on the control parameters and gains, in order to find the suitable values that allows a particular space mission to maximize the scientific mission time. Lastly, the algorithm developed for station-keeping of this particular problem can be extended to any general dynamical problem to develop a controlled environment.

Chapter 6

Bibliography

1) Y. Bai, J. D. Biggs, X. Wang, N. Cui. "A singular adaptive attitude control with active disturbance rejection". European Journal of Control. 2017

2) X. Bai, J. Junkins. "Modified Chebyshev-Picard Iteration Methods for Station-Keeping of Translunar Halo Orbits". *Mathematical Problems in Engineering.* 2012

3) J.D. Biggs, V.M. Becerra, S.J. Nasuto, V.F. Ruiz, W. Holderbaum. "A Search for Invariant Relative Satellite Motion". *Technical officer: Dario Izzo, Advanced Concepts Team (ESA/ESTEC).*

4) J. D. Biggs, H. C. Henninger, A. Narula. "Enhancing Station-Keeping Control With the Use of Extended State Observers". *Aerospace Science and Technology, Politecnico di Milano.* 2018

5) J.D. Biggs, C.R. McInnes. "Solar sail formation flying for deep space remote sensing". *Journal of Spacecraft and Rockets.* 2009

6) J.D. Biggs, C.R. McInnes, T. Waters. "Control of Solar Sail Periodic orbits in the Elliptic Three-Body Problem". *Journal of Guidance, Control and Dynamics.* 2009

7) S. Campagnola, M.W. Lo, P. Newton. "Subregions of motion and elliptic halo orbits in the elliptic restricted three-body". *Advance in Astronautical Sciences.* 2008

8) D. Cielaszyk, B. Wie. "New approach to halo orbit determination and control". *Journal of Guidance, Control, and Dynamics.* 2012

9) M. C. Eckstein. "Optimal station keeping by electric propulsion with thrust operation constraints". *Celestial Mechanics.* 1980

10) E. Eliason. "Clementine Mission". *Information from the CD-ROM VOLINFO.TXT file, assembled by many sources from E: Eliason.* 1994

11) R. Farquhar. "The utilization of halo orbits in advanced lunar operation". *NASA TN D-6365, GSFC, Greenbelt, Maryland.* 1971

12) F. Ferrari. "Non-Keplerian models for mission analysis scenarios about small solar system bodies". *PhD thesis, Politecnico di Milano.* 2016

13) D. Folta, F. Vaughn. "A survey of earth-moon libration orbits: Stationkeeping strategies and intra-orbit transfers". *AIAA/AAS Astrodynamics Specialist Conference and Exhibit.* 2004

14) D. Folta, M. Woodard, D. Cosgrove. "Stationkeeping of lissajous trajectories in the earth-moon system with applications to ARTEMIS". *Advances in the Astronautical Sciences, pp. 193-208.* 2011

15) D. C. Folta, M. Woodard, T. Pavlak, A. Haapala, K. Howell. "Earthmoon libration stationkeeping: Theory, modelling and operations". *Acta Astronautica, Vol. 94, Issue 1.* 2010

16) A. Garulli, A. Giannitrapani, M. Leomanni, F. Scortecci. "Autonomous station keeping for LEO missions with a hybrid continuous/impulsive electric propulsion system". $32^{nd} International Electric Propulsion Conference$.2011

17) G. Gomez, J. Llibre, R. Martinez, C. Simo. "Dynamics and Mission Design Near Libration Points. Vol. I Fundamentals: The Case of Collinear Libration Points". *World Scientific Monograph Series in Mathematics - Vol. 2*

18) S.C. Gordon. "Orbit Determination error analysis and station-keeping for libration point trajectories". *PhD thesis, Purdue University.* 1991

19) D.J. Grebow. "Generating Periodic Orbits in the Circular Restricted three-body problem with applications to Lunar South Pole Coverage". *PhD thesis.* Purdue University. 2006

20) A.F. Haapala, K.C. Howell. "Representations of higher-dimensional poincaré maps with applications to spacecraft trajectory design". *Acta Astronaut.* 2014

21) J. Han. "From pid to active disturbance rejection control". *IEEE Transactions on Industrial Electronic.* 2009

22) E. Hand. "Interplanetary small satellites come of age". *Science 361.6404.* 2018

23) K. Howell. "Families of orbits in the vicinity of the collinear libration points". *Journal of the Astronautical Sciences.* 2001

24) K.C. Howell. "Three dimensional, periodic, 'halo'orbits". *Celestial Mechanics.* 1984

25) K. Howell, T. Keeter. "Station-keeping strategies for libration point orbits: Target point and floquet mode approaches". *Advances in the Astronautical Sciences.* 1995

26) K. Howell, H. Pernicka. "Station-keeping method for libration point trajectories". *Journal of Guidance, Control, and Dynamics, Vol. 16, No. 1 (1993), pp. 151-159.* 2011

27) M. Kim, C. D. Hall. "Lyapunov and Halo orbits about L_2". AAS 01-324

28) A. Knutson, K. Howell. "Application of kanes method to incorporate attitude dynamics into the circular restricted three body problem". *AS/AIAA Space Flight Mechanics Meeting.* 2012

29) W. S. Koon. "Computation of Halo Orbit". Control and Dynamical Systems, Caltech Lesson

30) J.E. Kulkarni, M.E. Campbell. "Stabilization of spacecraft flight in halo orbits: An H_∞ approach". *IEEE Transactions on Control Systems Technology, Vol. 14, No. 3, pp.572-578.* 2012

31) Y. Liu, J. Heiligers, M. Ceriotti. "Loosely-displaced geostationary orbits with hybrid sail propulsion". Aerospace Science and Technology, 79. 2018

32) B. G. Marchand, K. C. Howell. "Control Strategies for Formation Flight in the Vicinity of the Libration Points". Journal of Guidance, Control and Dynamics. 2005

33) F.R. Moulton. *Periodic orbits.* 1920

34) A. Narula. "Fault-Tolerant Station keeping on Halo orbit in the Earth-Moon System". Master degree thesis, Politecnico di Milano. 2016

35) A. Narula, J.D. Biggs. "Fault-tolerant Station-keeping on Libration Point". *Journal of Guidance Control and Dynamics.* October 2017

36) K. Oguri, K.Kakihara, S. Campagnola, N. Ozaki, K. Oshima, T. Yamaguchi, R. Funase. "EQUULEUS Mission Analysis: Design of the Science Orbit Phase". 26th International Symposium on Space Flight Dynamics. 2017

37) M.T. Ozimek. "Low-Thrust Trajectory Design and Optimization". *PhD thesis, Purdue University.* 2010

38) T. Pavlak, K. Howell. "Strategy for Optimal, Long-Term Libration Point Orbit Stationkeeping in the Earth-Moon System". *AAS/AIAA Astrodynamics Specialist Conference.* 2012

39) H Poincaré. Les Méthodes Nouvelles de la Mécanique Céleste. 1899

40) V. Pyragas, K. Pyragas. "Act-and-wait time-delayed feedback control of autonomous systems". *Physics Letters A, Volume 382, Issue 8.* 2018

41) A. Rahmani, A. Jalali, S. Pourtakdoust. "Optimal approach to halo orbit control". *Proceedings of the AIAA Guidance, Navigation, and Control Conference and Exhibit, AIAA 2003-5748.* 2003

42) D L Richardson. "Analytic construction of periodic orbits about the collinear points". Celestial Mechanics. 1980

43) D. Sheng, X. Yang, H. R. Karimi. "Robust control for autonomous spacecraft evacuation with model uncertainty and upper bound of performance with constraints". *Mathematical Problems in Engineering.* 2013

44) V. Szebehely. "Theory of Orbits. The restricted problem of Three Bodies". Yale University, 1967

45) Thrustme "NPT30-I2 smart propulsion with iodine propellant" data-sheet

46) F. Topputo, M. Massari, J. Biggs, P. Di Lizia, D. A. Dei Tos, K. V. Mani, S. Ceccherini, V. Franzese, A. Cervone, P. Sundaramoorthy, S. Speretta, S. Mestry, R. Noomen, A. Ivanov, D. Labate, A. Jochemsen, R. Furfaro, V. Reddy, K. Jacquinot, R. Walker, J. Vennekens, A. Cipriano, D. Koschny. "LUMIO: Characterizing Lunar Meteoroid Impacts with a Cubesat". *69 th International Astronautical Congress (IAC), Bremen, Germany.* 2018

47) VACCO "ArgoMoon Propulsion System" data-sheet

48) F. Wang, X. Q. Chen, A. Tsourdos. "Sun–Earth L2 point formation control using polynomial eigenstructure assignment". *Acta Astronautica 76(3):26–36.* 2012

49) Wikipedia, last edited on 27 May 2020, `en.wikipedia.org/wiki/Schmitt_trigger`

50) B. Wong, R. Patil, A. Misra. "Attitude dynamics of rigid bodies in the vicinity of lagrangian points". *Journal of Guidance, Control, and Dynamics*. 2008

51) M. Xin, S. Balakrishnan. "A new method for sub-optimal control of a class of non-linear systems". *Optimal Control, Applications and Methods Vol. 26*. 2005

52) M. Zhu, H. Karimi, H. Zhang, Q. Gao, Y. Wang. "Active Disturbance Rejection Station-Keeping Control of Unstable Orbits around Collinear Libration Points". *Mathematical Problems in Engineering*. 2014

Ringraziamenti Speciali

Desidero cominciare a ringraziare i miei genitori, che mi hanno guidato nella scelta di questo percorso di studi e mi hanno supportato durante questi anni di intenso lavoro.
Un grazie a mio fratello, Giovanni, che mi sopporta sempre e che, nonostante le nostre diversità, rappresenta per me un grande pilastro.
Un forte ringraziamento è rivolto verso Sara, unica e insostituibile, la quale ha ascoltato più e più volte i miei pensieri e ragionamenti sulla tesi e che mi ha supportato durante i momenti più duri che ho affrontato.
Ringrazio inoltre i miei parenti, che rappresentano per me sempre una fonte di ispirazione, nonchè un punto fermo su cui contare sempre.
Un dovuto ringraziamento è rivolto ai miei amici, in ordine di incontro: Pinto, Loris, Fede, Tommy, Greta, Clara, Federico, Lesly, Pietro, Marco, Francesco, Danilo e Alessandro. Grazie ragazzi per questi anni passati insieme.